

# Bayesian Ambiguity Contraction-based Adaptive Robust Markov Decision Processes for Adversarial Surveillance Missions\*

Jimin Choi<sup>†</sup> and Max Z. Li<sup>‡</sup>  
University of Michigan, Ann Arbor, MI 48109, USA

Collaborative Combat Aircraft (CCAs) are envisioned to enable autonomous Intelligence, Surveillance, and Reconnaissance (ISR) missions in contested environments, where adversaries may act strategically to deceive or evade detection. These missions pose challenges due to model uncertainty and the need for safe, real-time decision-making. Robust Markov Decision Processes (RMDPs) provide worst-case guarantees but are limited by static ambiguity sets that capture initial uncertainty without adapting to new observations. This paper presents an *adaptive* RMDP framework tailored to ISR missions with CCAs. We introduce a mission-specific formulation in which aircraft alternate between movement and sensing states. Adversarial tactics are modeled as a finite set of transition kernels, each capturing assumptions about how adversarial sensing or environmental conditions affect rewards. Our approach incrementally refines policies by eliminating inconsistent threat models, allowing agents to shift from conservative to aggressive behaviors while maintaining robustness. We provide theoretical guarantees showing that the adaptive planner converges as credible sets contract to the true threat and maintains safety under uncertainty. Experiments under Gaussian and non-Gaussian threat models across diverse network topologies show higher mission rewards and fewer exposure events compared to nominal and static robust planners.

## Nomenclature

|          |   |  |
|----------|---|--|
| $S$      | = | Node set in the ISR graph              |
| $N(v)$   | = | Neighbor set of node $v$               |
| $S'$     | = | Two phase state space $(v, S), (v, M)$ |
| $\Theta$ | = | Threat type set                        |

\*A preliminary version of this paper titled "Adaptive Robust Markov Decision Process for Wide-Area Surveillance with Collaborative Combat Aircraft" (Control ID: 4355104) will be presented at the 2026 AIAA SciTech Forum, Orlando, FL, January 12-16, 2026 [1].

<sup>†</sup>Ph.D. Student, Department of Aerospace Engineering, AIAA Student Member

<sup>‡</sup>Assistant Professor, Department of Aerospace Engineering, Department of Civil and Environmental Engineering, Department of Industrial and Operations Engineering, AIAA Member

|   |   |  |
|---|---|--|
| $U_v^t$   | = | Credible threat set at node $v$            |
| $U_{s,a}^t$   | = | Local ambiguity set for $(s, a)$           |
| $b_{t,v}$   | = | Posterior belief at node $v$               |
| $o_{v,t}, z_{v,t}, \eta_{v,t}$  | = | Observation, exposure score, exposure flag |
| $e_t, d_t$  | = | Persistent and cumulative exposure states  |
| $n_t(v)$  | = | Novelty measure at node $v$                |
| $\gamma$  | = | Discount factor                            |
| $\alpha, \beta$   | = | Exposure decay and novelty decay           |
| $c_{\text{sense}}, c_{\text{move}}$   | = | Sensing and movement costs                 |
| $\lambda_{\text{imm}}, \lambda_{\text{pers}}, \lambda_{\text{cum}}, \lambda_{\text{nov}}$ | = | Reward weights                             |
| $p(o \mid a, \theta)$   | = | Observation distribution                   |
| $q(z \mid a, \theta)$   | = | Exposure score distribution                |
| $p_{\text{exp}}(a, \theta)$   | = | Exposure probability                       |
| $\phi_{s,a}$  | = | Map from threat type to transition kernel  |
| $r_{\text{sense}}, r_{\text{move}}$   | = | Sensing and movement rewards               |
| $V$   | = | Value function                             |
| $\pi_t$   | = | Policy at time $t$                         |
| $\mathcal{T}_r, \mathcal{T}_n$  | = | Robust and nominal Bellman operators       |

## I. Introduction

Collaborative Combat Aircraft (CCA) has been widely proposed as a key enabler in future air combat and surveillance operations, especially in contested or communication-denied environments [2, 3]. These platforms are expected to function autonomously or semi-autonomously, collaborating with other assets to perform complex tasks such as electronic warfare, precision targeting, and wide-area Intelligence, Surveillance, and Reconnaissance (ISR). This vision has been realized in the U.S. Air Force’s Next-Generation Air Dominance (NGAD) program, which positions CCAs as uncrewed force multipliers capable of performing distributed, high-risk missions in dynamic adversarial settings [4].

ISR has received growing attention among these roles due to its potential for distributed sensing and persistent situational awareness under limited centralized coordination. However, this optimistic outlook on autonomous ISR often underestimates the adversarial and deceptive nature of, and within real-world environments. Adversarial threat actors may employ mobile surface-to-air missile systems, intermittently activate radar sensors, or emit false signals to obscure their true positions and capabilities [5]. These behaviors challenge common and critical assumptions in autonomous planning: the availability of accurate models and stable dynamics. In such settings, ISR platforms operate

under partial observability and epistemic uncertainty about adversary behavior and environmental transitions.

At its core, this challenge represents a sequential decision-making problem under model uncertainty. Reinforcement learning (RL) has been widely explored as a solution, offering adaptability and the ability to generalize through data-driven policies. There has been increasing interest in using RL in aerospace applications such as autonomous navigation, flight control, and multi-agent mission planning [6–8]. However, RL methods typically require extensive exploration and lack safety guarantees, making them impractical for safety-critical missions [9]. As an alternative, Robust Markov Decision Processes (RMDPs) offer worst-case performance guarantees by optimizing over predefined ambiguity sets of transition models [10–12]. Nonetheless, conventional RMDP approaches rely on static ambiguity sets and do not incorporate new information gathered during mission execution, limiting their efficiency in dynamic or adversarial environments. In practice, when conducting ISR missions, as agents observe how threats sense, react, or reveal themselves, their understanding of the underlying adversarial model evolves. Reducing this uncertainty requires exploratory actions that may increase exposure, whereas acting conservatively limits the ability to refine the threat model.

This dynamic tension naturally gives rise to the exploration–exploitation dilemma specific to ISR missions, where agents must balance improving their understanding of adversarial behavior with maintaining safety and mission effectiveness. Recent studies on autonomous vehicle coordination in hazardous or uncertain domains have demonstrated the benefits of explicitly addressing this trade-off through uncertainty-aware and adaptive decision-making frameworks [13–15]. Although prior works offer practical strategies for handling exploration and risk, they do not explicitly formalize this trade-off within a robust sequential decision-making framework appropriate for ISR missions. Motivated by this gap, we propose an ISR mission–tailored adaptive RMDP framework that builds on the online robust planning formulation in [16] and naturally balances exploration and exploitation through uncertainty-aware policy adaptation. In doing so, agents reason over structured adversarial behaviors and dynamically adjust their strategies to maintain safety and coverage in contested environments.

The remainder of the manuscript is organized as follows. Section II provides the literature review and Section III presents the relevant background. Section V provides a detailed description of the mission setting and adaptive ISR mission strategy. Section VI introduces the adaptive robust planning framework, including the graph RMDP, Bayesian belief updates, and ambiguity contraction. Theoretical guarantees on convergence, safety, and asymptotic optimality are presented in Section VI.C. Simulation results across varying threat models and graph structures are shown in Section VII. Section VIII summarizes findings and outlines directions for future work.

## II. Literature Review

### A. Evolving ISR Missions under Uncertainty

ISR missions play a crucial role in maintaining tactical superiority in modern operations [17, 18]. In distributed missions with limited communications or in contested environments where electronic warfare is active, ISR platforms are expected to operate with a high level of autonomy and coordination [19]. Recent studies have increasingly focused on enhancing ISR effectiveness through adaptive and data-driven sensing with uncrewed aerial vehicles (UAVs). Learning-based approaches enable autonomous ISR systems to prioritize sensing tasks, allocate resources dynamically, and adapt mission objectives in response to evolving operational conditions [20]. In parallel, adaptive control frameworks are designed to sustain persistent surveillance under changing mission and environmental conditions, allowing multi-swarm UAV systems to reconfigure their coverage and maintain situational awareness over time [21]. These advances highlight the growing need for ISR systems that can make decisions and adapt autonomously amid uncertain threats and rapidly changing battle conditions.

Among these capabilities, persistent surveillance forms the core function of ISR operations, ensuring continuous situational awareness across time and space [22]. Achieving this persistence requires sustained coordination among diverse heterogeneous sensing assets. UAVs provide wide-area awareness but often lose visibility behind buildings or terrain, while uncrewed ground vehicles (UGVs) provide local ground-level sensing in those areas [23]. Recent studies have introduced cooperative UAV–UGV frameworks and energy-aware path planning methods to enhance mission endurance and maintain continuous surveillance in uncertain environments [24, 25]. Despite advances in multi-agent routing and coverage optimization, surveillance missions remain fundamentally constrained by environmental uncertainty and adversarial disruptions that threaten the continuity of observation [26]. Addressing this challenge requires robust decision-making frameworks that sustain persistent, reliable surveillance despite uncertainty.

### B. Applications of MDPs in Aviation

Decision-making in aviation involves sequential reasoning under uncertainty, and the MDP has become a fundamental framework for modeling such problems. MDP-based approaches have been applied across various aviation domains. For instance, MDP and partially observable MDP (POMDP) formulations have been employed to design automated collision avoidance systems that optimize between safety and flight efficiency [27–29]. In distributed ATM, multi-agent MDPs are used to coordinate advisories and resolve drone conflicts efficiently in real time [30–32]. Moreover, MDP-based frameworks support flight safety management systems that detect and mitigate loss-of-control scenarios during critical phases, such as takeoff [33], as well as aircraft routing strategy that optimizes trajectories under dynamic constraints [34].

Despite their wide range of applications, conventional MDP-based models typically rely on known, stationary transition probabilities, an assumption that rarely holds in real-world aviation settings [35]. When the true system

behavior diverges from these nominal models, policy performance can degrade or even become unstable [36]. To address this issue, RMDP formulations explicitly capture uncertainty in the transition dynamics and optimize decision policies that remain effective under worst-case realizations [11]. Such robustness represents a promising direction for safety-critical aviation missions, where reliable decisions in dynamic environments are essential for mission success and operational safety.

### C. Developments in RMDPs

In practice, the transition kernel of a Markov decision process is rarely known exactly, and policies optimized under estimated dynamics often exhibit substantial performance degradation when deployed out of sample [12]. To mitigate this sensitivity, the RMDP framework has emerged as a principled approach to improve generalization performance across uncertain environments [10, 11, 37]. Most existing studies on RMDPs focus on the offline setting, where the decision maker seeks to infer an optimal policy from a fixed dataset of trajectories generated by an unknown behavior policy, without further interaction with the environment [38]. In this regime, pessimistic value estimation has proven to yield statistically efficient algorithms for offline reinforcement learning [39]. One study introduces an online robust planning approach that achieves sublinear regret by incorporating optimism into the policy update under rectangular uncertainty, marking an early effort toward adaptive robust decision-making [16].

However, when data are collected online, the distribution generating the data typically differs from the distribution that determines policy performance—a discrepancy known as the sim-to-real gap in reinforcement learning [40]. Addressing this gap requires algorithms that explicitly trade off exploration and robustness to uncertainty in the transition kernel. While recent studies have begun to extend the RMDP framework to online learning, these methods either rely on an alternative notion of robust regret [41] or require a technical loop-free assumption on the structure of the MDP [16]. To summarize, the loop-free assumption excludes cyclic dynamics that arise naturally in most practical Markov decision processes. A key open challenge lies in designing algorithms that adaptively learn policies under evolving uncertainty while ensuring sublinear regret with respect to the true data-generating process.

## III. Preliminaries

We consider an infinite-horizon Markov Decision Process (MDP) given by a six-tuple  $(\mathcal{S}, \mathcal{A}, P, r, \gamma, s_0)$  comprising of a finite state space  $\mathcal{S} = \{1, \dots, S\}$ , a finite action space  $\mathcal{A} = \{1, \dots, A\}$ , a transition kernel  $P : \mathcal{S} \times \mathcal{A} \rightarrow \Delta(\mathcal{S})$ , a reward-per-stage function  $r : \mathcal{S} \times \mathcal{A} \rightarrow \mathbb{R}$ , a discount factor  $\gamma \in (0, 1)$ , and an initial state  $s_0 \in \mathcal{S}$ . Note that  $(\mathcal{S}, \mathcal{A}, P, r, \gamma, s_0)$  describes a controlled discrete-time stochastic system, where the state at time  $t$  and the action applied at time  $t$  are denoted as random variables  $S_t$  and  $A_t$ , respectively. If the system is in state  $s_t \in \mathcal{S}$  at time  $t$  and action  $a_t \in \mathcal{A}$  is applied, then an immediate reward  $r(s_t, a_t)$  is incurred, and the system moves to state  $s_{t+1}$  at time  $t + 1$  with probability  $P(s_{t+1}|s_t, a_t)$ . We denote the underlying probability distribution over all of the possible state and action

sequences as  $\mathbb{P}_\pi^P$ .

We denote the expectation operator with respect to  $\mathbb{P}_\pi^P$  by  $\mathbb{E}_\pi^P[\cdot]$ . Note that the stochastic process  $\{S_t\}_{t=0}^\infty$  is a time-homogeneous Markov chain under  $\mathbb{P}_\pi^P$  with transition probabilities  $\mathbb{P}_\pi^P(S_{t+1} = s' | S_t = s) = \sum_{a \in \mathcal{A}} P(s'|s, a)\pi(a|s)$ . Throughout this paper, we assess the desirability of a policy by its expected net present value, which is captured directly in the definition of the value function. The value function  $V_\pi^P \in \mathbb{R}^S$  corresponding to a transition kernel  $P$  and a stationary policy  $\pi$  is defined through

$$V_\pi^P(s) = \lim_{T \rightarrow \infty} \mathbb{E}_\pi^P \left[ \sum_{t=0}^T \gamma^t r(S_t, A_t) \mid S_0 = s \right].$$

The policy evaluation problem consists in evaluating the value function  $V_\pi^P(s)$  for a fixed policy  $\pi$  and initial state  $s$ , whereas the policy improvement problem seeks a policy that maximizes  $V_\pi^P(s)$ .

In practice, the transition kernel  $P$  is not known precisely *a priori* [12]. Moreover, transition models estimated from limited data are highly sensitive to misspecification, and small estimation errors can significantly degrade policy performance [11]. Thus, it is natural to use the RMDP framework to find a policy that maintains performance across a set of plausible transition kernels. Under the RMDP framework, we suppose that the transition kernel  $P$  is only known to belong to an ambiguity set  $\mathcal{P} \subseteq \Delta(\mathcal{S})^{S \times A}$ , where  $\Delta(\mathcal{S})$  denotes the probability distributions over states. We assess the desirability of a policy by its *worst-case* expected value. The worst-case value function  $V_\pi^\star \in \mathbb{R}^S$  associated with a given policy  $\pi$  and an ambiguity set  $\mathcal{P}$  is then defined through

$$V_\pi^\star(s) = \min_{P \in \mathcal{P}} V_\pi^P(s). \quad (1)$$

The *robust policy evaluation problem* then consists in evaluating the worst-case value function  $V_\pi^\star(s)$  for a fixed policy  $\pi$  and initial state  $s$ , and the *robust policy improvement problem* aims to solve

$$\max_{\pi \in \Pi} \min_{P \in \mathcal{P}} V_\pi^P(s). \quad (2)$$

The structure of the ambiguity set  $\mathcal{P}$  largely determines the difficulty of solving the robust policy evaluation and optimal policy computation. These problems become relatively easy if the ambiguity set is rectangular (see Definition 1) because dynamic programming principle holds for these types of RMDP problems. Under the rectangularity assumption of the ambiguity set, we construct the robust Bellman operator by replacing the expectation over a fixed transition model with the worst-case expectation over the set of plausible transition kernels. This modification still preserves contraction and fixed-point properties that are standard in the literature [12]. Intuitively, contraction ensures that repeated Bellman updates progressively bring value estimates closer together rather than diverging, while the fixed-point

property guarantees that this process converges to a unique stable solution representing the long-run value of each state. We introduce the formal definition of rectangular ambiguity sets below.

**Definition 1** (Rectangular ambiguity sets). *A set  $\mathcal{P} \subseteq \Delta(\mathcal{S})^{S \times \mathcal{A}}$  of transition matrices is called*

- (i)  *$(s, a)$ -rectangular if  $\mathcal{P} = \prod_{(s,a) \in S \times \mathcal{A}} \mathcal{P}_{s,a}$  for some  $\mathcal{P}_{s,a} \subseteq \Delta(\mathcal{S})$ ,  $(s, a) \in S \times \mathcal{A}$  [10, 11];*
- (ii)  *$s$ -rectangular if  $\mathcal{P} = \prod_{s \in S} \mathcal{P}_s$  for some  $\mathcal{P}_s \subseteq \Delta(\mathcal{S})^{\mathcal{A}}$ ,  $s \in S$  [37].*

Here,  $\Delta(\mathcal{S})$  denotes the probability distributions over next states, and  $\Delta(\mathcal{S})^{\mathcal{A}}$  is the Cartesian product of  $\mathcal{A}$  copies of  $\Delta(\mathcal{S})$ , assigning one transition distribution to every action at state  $s$ . Under  $(s, a)$ -rectangularity, uncertainty is modeled independently at each state–action pair, whereas under  $s$ -rectangularity it is specified at the state level and shared across actions taken at that state.

Such independence structures arise naturally in many real systems. In persistent surveillance, detection at each location is primarily determined by local environmental conditions, line-of-sight, and sensor posture, yielding probabilistic coverage models driven by local geometry and visibility [42]. In multi-robot coverage, sensing performance within an operating region is modeled with respect to the robot’s configuration and the environment in that region, consistent with decentralized, region-based coverage formulations [43].

In our ensuing discussions, we will consider RMDPs with  $(s, a)$ -rectangular sets. Recall that  $(s, a)$ -rectangularity requires that the adversary selects the next-state distribution independently for each state–action pair. By contrast, under  $s$ -rectangularity, the adversary’s choice of the next-state distribution may depend on the decision maker’s entire policy. Thus,  $(s, a)$ -rectangularity grants the adversary greater flexibility, leading to a more conservative optimal robust policy for the decision maker as compared to the  $s$ -rectangularity case.

## IV. Contributions of Work

The main contributions of our work are as follows:

- *Mission-specific RMDP formulation:* We develop a two-phase, graph-based RMDP that captures the operational structure of CCA conducting ISR missions. Our model captures key operational factors such as spatial constraints, exposure risks, and sensing limitations, allowing ISR missions to be viewed as sequential decision-making problems that balance information gathering and survivability.
- *Adaptive online robust planning:* We tailor and extend the adaptive RMDP framework [16] for ISR missions by integrating Bayesian inference–based ambiguity contraction and relaxing the loop-free assumption. This mechanism refines local uncertainty using online sensing data, allowing policies to transition naturally from conservative to aggressive behavior and revealing an inherent trade-off between robustness and efficiency.
- *Theoretical foundation for adaptive robustness:* We provide formal guarantees for the proposed adaptive robust planner, including almost-sure convergence of time-varying robust Bellman operators, finite-time safety bounds

under rectangular uncertainty, and asymptotic optimality as credible sets with threat hypotheses consistent with local observations contract to the true threat type. These results establish that the proposed method remains conservative under uncertainty while recovering optimal performance as information accumulates.

- *Simulation-based evaluation:* We validate the proposed framework through multi-stage simulations that examine three key aspects: baseline convergence and stability, scalability with increasing graph size and threat diversity, and generalization to non-Gaussian threat distributions. In Experiment 1, the adaptive planner achieved similar ISR observation rewards to the nominal baseline while reducing exposure events by 84%, with the static robust planner serving as a conservative lower bound for our planner. The results consistently demonstrate improved ISR efficiency and reduced exposure compared with nominal and static robust baselines.

## V. Problem Statement

### A. Mission Scenario

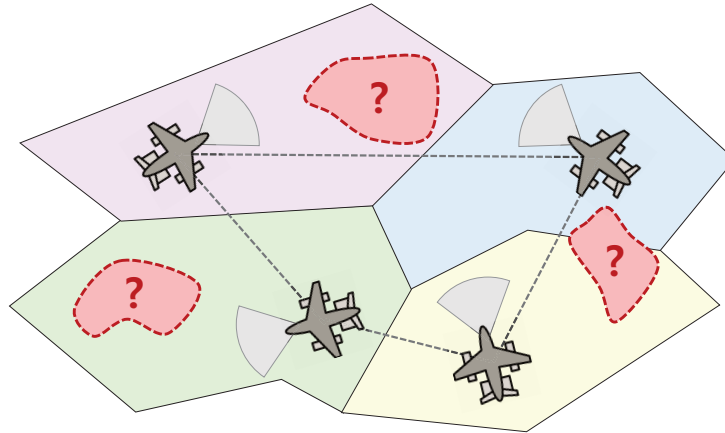


**Fig. 1 Mission-level concept for decentralized ISR missions with CCAs.** Each aircraft conducts surveillance within an assigned region under local threat uncertainty. Colored polygons indicate example regional areas, red dashed zones mark uncertain threat locations, and aircraft icons with sensing arcs illustrate sensing coverage.

Autonomous ISR missions in contested environments require aircraft to monitor large geographic regions that may contain uncertain adversarial threats. These threats can exhibit a wide range of adversarial behaviors, often acting strategically to expose or deceive ISR aircraft operating in the area. While the exact threat behavior is unknown, each ISR aircraft maintains a set of known *prototype* models representing plausible adversary strategies. This is feasible because adversary tactics often follow a few recurring patterns, such as aggressive radar use or passive sensing. We assume that, based on prior intelligence, these patterns are encoded as prototype models and installed in each aircraft's reasoning system.

**Definition 2** (Prototype). A prototype is a predefined transition model that represents one plausible adversary strategy



*inferred from prior knowledge. Each prototype captures a distinct pattern in how the adversary senses, reacts, or engages with ISR aircraft (e.g., continuous radar emission, intermittent activation, passive monitoring). The true adversary behavior is assumed to coincide with one element in this finite set, each corresponding to a full transition kernel. At each node in the environment, the agent maintains a credible set containing the prototype models that remain consistent with the observed threat responses at that location.*

In this setting, we introduce a team of CCAs operated in a coordinated manner to monitor the environment while managing uncertainty and avoiding adversarial threats. Each aircraft operates under model uncertainty and decides its trajectory, sensing strategy, and threat-avoidance policy in real time, without access to the ground truth adversary model. The key challenge is operating CCAs safely in an environment with potential threats while maximizing the information gain achievable through distributed sensing. The mission objective is to maximize the reliable collection of ISR information across the operational area while maintaining safety under uncertain, structured threat dynamics.

Figure 1 illustrates the mission-level concept: a surveillance task is carried out by a fleet of CCAs, each assigned to a portion of the operational space. Threats, represented by uncertain adversarial behavior, may exist anywhere within the region and follow one of several known behavioral prototypes. Each aircraft autonomously selects actions and sensing directions while sharing threat information.

**Scope of This Study.** While the mission concept in Figure 1 involves a team of CCAs, this work does not directly model multi-agent coordination or inter-regional task allocation. Instead, we focus on the decision-making problem of a single autonomous flight operating within its assigned region, assuming that the overall area has been pre-divided among aircraft before mission execution. Each flight independently performs its ISR task under local threat uncertainty, applying the proposed adaptive robust framework to its region. This formulation serves as a foundational step toward future research (see Section VIII.B) on multi-agent coordination, dynamic region reassignment, and human pilot–CCA teaming under uncertainty.

## **B. Proposed Adaptive RMDP Framework**

To address this problem, we propose an online adaptive RMDP framework in which uncertainty over adversary behavior is represented through node-wise credible sets  $U_v^t$ . Each credible set is initialized as  $U_v^0 = \Theta$ , which contains all prototype threat models based on prior knowledge. These credible sets induce the corresponding transition ambiguity sets  $U_{s,a}^t$  through a fixed mapping  $U_{s,a}^t = \phi_{s,a}(U_v^t)$ , so that at the beginning of the mission the ambiguity sets cover the entire range of transition models consistent with the prototype set. Each aircraft therefore begins with a conservative strategy that assumes the worst-case threat among known prototypes. Over time, local observations enable each aircraft to eliminate incompatible prototype models, gradually refining its belief and adapting its behavior. As the credible sets shrink, the induced ambiguity sets contract accordingly, enabling a transition from a cautious policy to more confident

and efficient ISR operations.

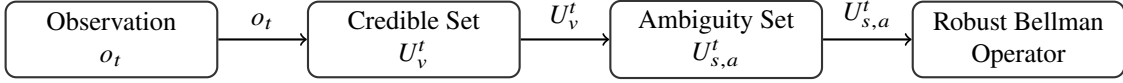


**Fig. 2 Information flow in the adaptive RMDP framework. Observations refine credible sets, which induce transition ambiguity sets used by the robust Bellman operator.**

**Table 2 Credible sets and ambiguity sets in the adaptive RMDP.**

|                    | Credible Set $U_v^t$                        | Ambiguity Set $U_{s,a}^t$                             |
|--------------------|---|---|
| <i>Definition</i>  | Plausible threat types at node $v$          | Transition models induced by $U_v^t$ via $\phi_{s,a}$ |
| <i>Uncertainty</i> | Model uncertainty from limited observations | Transition uncertainty captured in the RMDP           |
| <i>Update</i>      | Shrinks from posterior updates and pruning  | Contracts through $U_{s,a}^t = \phi_{s,a}(U_v^t)$     |
| <i>Usage</i>       | Determines remaining prototype hypotheses   | Used in the robust Bellman operator                   |

In the early phase of the mission, all aircraft operate conservatively, using robust policies induced by the initial credible sets, which contain all prototype threat models. As the mission progresses, the system adapts dynamically to eliminate unlikely prototype models, gradually refining both its beliefs and the associated ambiguity sets. This results in progressively more targeted and efficient ISR mission trajectories. This gradual shift from cautious to efficient behavior reflects a continuous exploration–exploitation trade-off achieved through policy refinement: Initially, aircraft act conservatively under large model uncertainty. As they gain confidence through ongoing observations, their policies become increasingly refined, enabling more efficient ISR mission without compromising robustness.

## VI. Methodology

This section formalizes the adaptive robust planner used in our ISR mission scenario. We first specify the graph implementation to the RMDP notation from Section III, then specify observation and exposure models, the reward decomposition, and the robust and nominal value-iteration operators. We next introduce the adaptive update rule in which Bayesian posteriors shrink the node-wise credible sets and, through the mapping  $\phi_{s,a}$ , the induced transition ambiguity sets. Finally, we present the theory establishing the convergence and safety guarantees of the proposed adaptive robust planner.

### A. Graph-based Robust RMDP for ISR

ISR missions involve sequential decision-making under uncertainty, where the agent balances information gathering with exposure risk. To model this setting formally, we represent the operational environment as a graph-structured RMDP. As illustrated in Figure 3, each node corresponds to a spatial location with an unknown latent threat type, and transitions occur through movement along the graph edges. The aircraft takes sensing actions when located at a node and movement actions along the graph edges to navigate between adjacent surveillance locations.

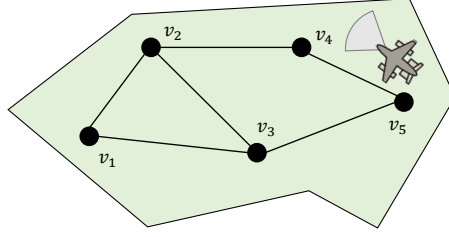


**Fig. 3** A zoomed-in view of a single ISR operation region from Figure 1. The polygon shows one aircraft's assigned area, where each node represents a surveillance point with its own threat type, and edges define feasible movements. The aircraft performs sensing-based actions at nodes and movement actions along edges.

### 1. Graph RMDP with Two-Phase States

In our model, each node  $v$  in the graph represents a state  $s \in \mathcal{S}$ . The node-wise ambiguity sets  $U_{s,a}^t$  correspond to local subsets of the global transition ambiguity set  $\mathcal{P}_t$ . We consider an undirected graph  $G = (\mathcal{S}, \mathcal{E})$ , where the node set is  $\mathcal{S} = \{0, \dots, S-1\}$  and each node  $v$  has neighbors  $\mathcal{N}(v) = \{u \in \mathcal{S} : (v, u) \in \mathcal{E}\}$ . Each node  $v$  is assigned an unknown threat type  $\theta_v \in \Theta = \{1, \dots, n_\theta\}$ , and the system evolves in alternating *sense* and *move* phases. We lift the original state space  $\mathcal{S}$  to a two-phase version

$$\mathcal{S}' = \{(v, S'), (v, M') : v \in \mathcal{S}\}. \quad (3)$$

At sense states  $(v, S')$  the action set is  $\mathcal{A}_S = \{A, B, C, \dots\}$ , and at move states  $(v, M')$  the action set is  $\mathcal{A}_{M'}(v) = \mathcal{N}(v)$  if  $\mathcal{N}(v) \neq \emptyset$  and  $\mathcal{A}_{M'}(v) = \{v\}$  otherwise. This two-phase design reflects real ISR missions, in which remaining in one place for extended periods increases the risk of exposure, defined as the event that the aircraft becomes observable to adversarial sensors. Alternating between sensing and movement prevents this buildup of risk and reduces prolonged exposure within a single region.

### 2. Observation and Exposure Models

When taking a sense action  $a \in \mathcal{A}_{S'}$  at node  $v$ , the agent conducts local reconnaissance and receives a scalar observation  $o_v$  that quantifies the information gained from that area.

$$o_{v,t} \sim p(o | a_t, \theta_v), \quad (4)$$

where  $p(o | a, \theta_v)$  denotes the observation distribution conditioned on the sensing action and the local threat type. In this context, exposure refers to the ISR aircraft being detected or otherwise compromised by the local threat. The agent independently samples an exposure score

$$z_{v,t} \sim q(z | a_t, \theta_v), \quad (5)$$

where  $q(z | a, \theta_v)$  represents the exposure score distribution. This score induces a binary exposure event

$$\eta_{v,t} = \mathbb{1}[z_{v,t} > \tau_\eta], \quad (6)$$

for a fixed threshold  $\tau_\eta > 0$ . The corresponding exposure probability is given by

$$p_{\text{exp}}(a, \theta) = \int_{\tau_\eta}^{\infty} q(z | a, \theta) dz, \quad (7)$$

which represents the probability that the exposure score exceeds the threshold  $\tau_\eta$ . Both distributions  $p$  and  $q$  depend on the prior knowledge of the environment available before the mission begins, and the observation and exposure processes are assumed to be independent given  $a$  and  $\theta_v$ .

### 3. Reward Model

We design the reward to capture four operational factors. Sensing utility measures how informative an observation is at a location, reflecting the surveillance value gained from the action. Exploration novelty encourages visiting less-explored nodes to expand situational awareness rather than repeatedly sampling familiar areas. Exposure risk penalizes actions that increase the chance of detection or compromise, accounting for both immediate and persistent effects of past exposure. Finally, operational cost reflects resource burdens such as fuel usage or reduced endurance. We express the sensing reward as

$$r_{\text{sense}}(v_t, a_t, \theta_v) = r_{\text{obs}}(v_t, a_t, \theta_v) + r_{\text{nov}}(v_t) + r_{\text{haz}}(\eta_{v,t}) - c_{\text{sense}}(a_t). \quad (8)$$

The individual components are defined as follows:

$$\begin{aligned} r_{\text{obs}}(v_t, a_t, \theta_{v_t}) &= \mathbb{E}[u(o_{v_t,t}) | a_t, \theta_{v_t}], \\ r_{\text{nov}}(v_t) &= \lambda_{\text{nov}} n_t(v_t), \\ r_{\text{haz}}(\eta_{v,t}) &= \lambda_{\text{imm}}(-\eta_{v,t}) + \lambda_{\text{pers}}(-e_t) + \lambda_{\text{cum}}(-\log(1 + d_t)), \\ c_{\text{sense}}(a_t) &\geq 0. \end{aligned} \quad (9)$$

The observation reward  $r_{\text{obs}}(v_t, a_t, \theta_v)$  quantifies the expected sensing gain under latent threat type  $\theta_v$ . The variable  $e_t \in [0, 1]$  represents a penalty carried over from a previous exposure event. It decays over time at a rate  $\alpha \in (0, 1)$ , which modulates the persistence of exposure risk through the term  $-\lambda_{\text{pers}}e_t$  in the reward, but resets to 1 whenever a new exposure occurs. The cumulative count  $d_t$  records the number of exposures, updated as  $d_{t+1} = d_t + \eta_{v,t}$ . The novelty map  $n_t(v) \geq 0$  increases when a node has not been visited recently. We implement it as an exponential moving

average of the time since the last visit,

$$n_{t+1}(v) = \beta n_t(v) + (1 - \beta)(t - t_{\text{last}}(v)), \quad (10)$$

where  $t_{\text{last}}(v)$  denotes the most recent visit time and  $\beta \in (0, 1)$  controls the decay rate. An exponential moving average avoids abrupt jumps that occur when a node is visited once after a long absence. This smooth update provides a simple, stable measure of how long since the node was visited.

In the move states, the reward is defined as

$$r_{\text{move}}(v_t \rightarrow v_{t+1}) = -c_{\text{move}} + \lambda_{\text{nov}} n_t(v_{t+1}) + \lambda_{\text{pers}}(-e_t) + \lambda_{\text{cum}}(-\log(1 + d_t)). \quad (11)$$

Each term plays a distinct functional role. The novelty bonus  $r_{\text{nov}}(v_t) = \lambda_{\text{nov}} n_t(v_{t+1})$  encourages exploration of less-visited regions. The hazard term aggregates exposure penalties across three timescales: an immediate penalty  $-\lambda_{\text{imm}} \eta_{v,t}$  for direct exposure, a persistent penalty  $-\lambda_{\text{pers}} e_t$  for sustained exposure, and a cumulative penalty  $-\lambda_{\text{cum}} \log(1 + d_t)$  for repeated exposures. Finally, the sensing and movement costs  $c_{\text{sense}}(a)$  and  $c_{\text{move}}$  introduce operational penalties that discourage inefficient sensing or movement, respectively. The weighting parameters  $\lambda$  control the trade-off between exploration and risk in the adaptive planner.

#### 4. Threat Models and Ambiguity Sets

$\mathcal{P}_t$  denotes the global transition ambiguity set at time step  $t$ . Recall that in our formulation, uncertainty is represented node-wise through posterior credible sets  $U_v^t \subseteq \Theta$ . Each element  $\theta \in \Theta$  corresponds to a distinct threat prototype that governs sensing outcomes and exposure statistics. The credible set  $U_v^t$  therefore captures the set of threat types that remain plausible for node  $v$  under the current posterior. For any state-action pair  $(s, a)$  associated with node  $v$ , these credible sets are mapped to local transition ambiguity sets through the continuous map  $U_{s,a}^t = \phi_{s,a}(U_v^t)$ , and the overall transition ambiguity takes the rectangular form  $\mathcal{P}_t = \prod_{(s,a)} U_{s,a}^t$ . Following the standard RMDP literature [10], these local sets are assumed independent across nodes, consistent with an  $(s, a)$ -rectangular uncertainty structure.

The credible sets define a stage-wise robust sensing reward. For any sense action  $a \in \mathcal{A}_S$  at node  $v$ , we set

$$\tilde{r}_{\text{rob}}(v, a, U_v^t) = \min_{\theta \in U_v^t} \left[ \mathbb{E}_{p(o|a,\theta)}[o] + \lambda_{\text{imm}}(-p_{\text{exp}}(a, \theta)) \right] - c_{\text{sense}}(a), \quad (12)$$

where the minimization provides a conservative estimate of the expected sensing reward consistent with the worst-case threat realization within the credible set  $U_v^t$ . When  $U_v^t = \{\hat{\theta}_v\}$ , the credible set collapses to a singleton, meaning that only one threat hypothesis remains consistent with past observations at node  $v$ , and the robust surrogate reduces to the

nominal reward

$$\tilde{r}_{\text{nom}}(v, a) = \mathbb{E}_{p(o|a, \hat{\theta}_v)}[o] + \lambda_{\text{imm}}(-p_{\text{exp}}(a, \hat{\theta}_v)) - c_{\text{sense}}(a). \quad (13)$$

This nominal surrogate corresponds to planning under a single estimated threat type, without accounting for uncertainty in  $\theta_v$ . This surrogate serves as the local reward model used in the robust Bellman updates.

## B. Adaptive RMDP for ISR

This section describes the adaptive planning mechanism that integrates robust value iteration with Bayesian inference and posterior-driven ambiguity contraction. The resulting loop adaptively refines node-wise credible sets  $U_v^t$  and the induced transition ambiguity sets  $U_{s,a}^t$ , while replanning under updated novelty maps  $n_t(v)$ .

### 1. Bellman Operators and Value Iteration

Let  $V : S' \rightarrow \mathbb{R}$  denote the value function over the two-phase state space. During each Bellman update, auxiliary quantities that depend on visit history or past exposure, such as the novelty map  $n_t(v)$ , the persistent exposure level  $e_t$ , and the cumulative exposures  $d_t$ , are considered fixed at the current time step.

$$(\mathcal{T}_r V)(v, S') = \max_{a \in \mathcal{A}_{S'}} \left\{ \tilde{r}_r(v, a, U_v^t) + \lambda_{\text{nov}} n_t(v) + \gamma V(v, M') \right\}, \quad (14)$$

$$(\mathcal{T}_r V)(v, M') = \max_{u \in \mathcal{A}_{M'}(v)} \left\{ -c_{\text{move}} + \lambda_{\text{nov}} n_t(u) + \gamma V(u, S') \right\}. \quad (15)$$

The nominal operator  $\mathcal{T}_{n'}$  is defined analogously to  $\mathcal{T}_r$ , with the robust surrogate  $\tilde{r}_r$  replaced by its nominal counterpart  $\tilde{r}_{n'}$ . Intuitively,  $\mathcal{T}_r$  performs a worst-case backup over all plausible threat realizations, while  $\mathcal{T}_{n'}$  corresponds to standard Bellman updates under a single estimated type. Both operators are  $\gamma$ -contractions under the supremum norm, ensuring that repeated application of the Bellman update,

$$V_{k+1} = \mathcal{T}_\xi V_k, \quad \xi \in \{r', n'\}, \quad (16)$$

converges to a unique fixed point  $V_\xi^*$ . The resulting value function defines a greedy policy  $\pi_\xi^*$  that is stationary and optimal with respect to the chosen operator. The contraction property further guarantees stable convergence even when ambiguity sets evolve adaptively over time.

The robust Bellman operator implicitly guards against observation and exposure uncertainty by optimizing for the worst-case threat realization within each local ambiguity set. This guarantees a conservative value estimate that bounds mission risk even under distributional shifts in sensing or exposure statistics. This property is particularly desirable in ISR mission contexts, where estimated threat distribution may differ from the true underlying distribution due to deception or sparse and imperfect observations.

## 2. Bayesian Belief Update and Shrinkage of Credible Sets and Ambiguity Sets

At each sensing step at node  $v$ , the agent maintains a belief distribution  $b_{t,v}$  over possible threat types, which is updated according to the observation likelihood as

$$b_{t+1,v}(\theta) = \frac{b_{t,v}(\theta) p(o_t | a_t, \theta)}{\sum_{\theta' \in \Theta} b_{t,v}(\theta') p(o_t | a_t, \theta')}, \quad (17)$$

where  $p(o_t | a_t, \theta)$  denotes the observation likelihood function associated with action  $a_t$  and threat type  $\theta$ . The credible set is then refined according to the posterior confidence rule

$$U_v^{t+1} = \begin{cases} \arg \max_{\theta} b_{t+1,v}(\theta) & \text{if } \max_{\theta} b_{t+1,v}(\theta) \geq \rho_{\text{lock}}, \\ \{\theta \in U_v^t : b_{t+1,v}(\theta) \geq \varepsilon_{\text{prune}}\}, & \text{otherwise.} \end{cases} \quad (18)$$

The rule commits to the most probable threat type once the posterior confidence exceeds the locking threshold, while pruning low-probability hypotheses from the credible set otherwise. Specifically, posterior log-gaps between the  $i$ -th and  $j$ -th most probable types at node  $v$  are evaluated as

$$g_{i,j}(v) = \log \left( \frac{b_{t+1,v}(\theta_{(i)})}{b_{t+1,v}(\theta_{(j)})} \right), \quad (19)$$

where  $\theta_{(i)}$  and  $\theta_{(j)}$  denote posterior hypotheses ranked by their probabilities in descending order. When  $g_{i,j}(v)$  exceeds pre-defined thresholds, the lower-probability hypotheses are removed from  $U_v^t$ . Models with persistently low posterior mass reflect threat behaviors that are consistently ruled out by the observed sensing outcomes. Because each credible set  $U_v^t$  induces the transition ambiguity sets  $U_{s,a}^t = \phi_{s,a}(U_v^t)$ , any reduction of  $U_v^t$  necessarily produces a contraction of the corresponding ambiguity sets. Crucially, no additional exploratory actions are needed: routine surveillance naturally produces observations that distinguish plausible hypotheses from implausible ones. As a result, ambiguity reduction occurs through ongoing surveillance, enabling the aircraft to become less conservative over time without compromising safety. The SHRINK operator in Algorithm 1 implements exactly this posterior-based pruning rule.

## 3. Adaptive Robust Planning Loop

The adaptive robust planner replans every  $K$  steps based on the current visit statistics and ambiguity sets, as outlined in Algorithm 1. This loop implements a closed-form interaction between inference and planning: Bayesian updates refine node-wise beliefs, posterior-driven shrinkage tightens local ambiguity sets, and periodic robust replanning ensures consistent adaptation to evolving situational awareness. The robust value iteration guarantees that, even during early uncertain phases, the policy remains safe against the worst-case realizations within each local ambiguity set.

As uncertainty diminishes and local ambiguity sets collapse to singletons, the adaptive robust planner smoothly

---

**Algorithm 1** Adaptive Robust Planning for ISR

---

```
1: Initialize uniform beliefs  $b_{0,v}(\theta) = 1/|\Theta|$  and credible sets  $U_v^0 = \Theta$  for all  $v \in \mathcal{S}$  ▷  $|\Theta|$  is the cardinality of  $\Theta$ 
2: Initialize exposure variables  $e_0 = 0$ ,  $d_0 = 0$ , and novelty map  $n_0(v) = 0$  for all  $v$ 
3: for  $t = 0, 1, \dots, T - 1$  do
4:   if  $t \equiv 0 \pmod{K}$  then
5:     Solve robust value iteration with  $U_v^t$  and current novelty map  $n_t(v)$  to obtain policy  $\pi_t$ 
6:   end if
7:   Observe current state  $(v_t, S')$  and take sense action  $a_t = \pi_t(v_t, S')$ 
8:   Sample observation  $o_t \sim p(o | a_t, \theta_{v_t})$  and exposure score  $z_t \sim q(z | a_t, \theta_{v_t})$ 
9:   Set exposure indicator  $\eta_{v,t} = \mathbb{1}[z_t > \tau_\eta]$ 
10:  Update belief:  $b_{t+1,v_t}(\theta) = \frac{b_{t,v_t}(\theta) p(o_t | a_t, \theta)}{\sum_{\theta' \in \Theta} b_{t,v_t}(\theta') p(o_t | a_t, \theta')}$ 
11:  Update exposure variables:  $e_{t+1} = \max\{\alpha e_t, \eta_{v,t}\}$ ,  $d_{t+1} = d_t + \eta_{v,t}$ 
12:  Update novelty map  $n_{t+1}(v)$  based on visit recency according to (10)
13:  Update credible set:  $U_{v_t}^{t+1} \leftarrow \text{SHRINK}(U_{v_t}^t, b_{t+1,v_t})$ ,  $U_v^{t+1} \leftarrow U_v^t$  for  $v \neq v_t$ 
14:  Update induced ambiguity sets:  $U_{s,a}^{t+1} \leftarrow \phi_{s,a}(U_v^{t+1})$  for all state-action pairs  $(s, a)$  associated with  $v$ 
15:  Move according to  $u_t = \pi_t(v_t, M')$  and set next state  $(u_t, S')$ 
16: end for
```

---

transitions toward nominal behavior, recovering standard value iteration in the limit. In particular, as ambiguity sets shrink and converge to singletons, the planner asymptotically recovers the nominal value function  $V_{\text{nom}}^*$ , ensuring policy consistency with standard MDP solutions. This gradual transition preserves robustness during uncertainty while avoiding overly conservative behavior in well-understood regions.

This structure aligns naturally with ISR mission requirements, where agents need to balance information gathering and exposure risk under uncertain environmental conditions. By coupling belief refinement with robust decision-making, the planner maintains operational safety while efficiently allocating limited sensing opportunities, resulting in adaptive behaviors consistent with practical ISR mission dynamics. Together, these components enable the planner to gradually shift from conservative exploration to confident exploitation as uncertainty diminishes, maintaining robustness throughout the mission.

### C. Theoretical Properties

We establish guarantees for the adaptive robust planner. Throughout, we work with finite state and action sets. The lifted state space  $\mathcal{S}'$  created in the two-phase formulation is also finite.

#### 1. Assumptions and Regularity Conditions

**Assumption 1** (Discounting and bounded rewards). *The discount factor satisfies  $\gamma \in (0, 1)$ . Per-step rewards and costs are uniformly bounded and measurable. Any cumulative exposure penalty is bounded so that  $\sup_{s,a} |r(s, a)| < \infty$ .*

**Assumption 2** ( $(s, a)$ -rectangular uncertainty and contraction). *For any  $(s, a)$ -rectangular family of ambiguity sets  $\{U_{s,a} \subseteq \Delta(\mathcal{S}')\}$ , where  $\Delta(\mathcal{S}')$  denotes the probability simplex over the state space  $\mathcal{S}'$  at the next time step, the robust*



*Bellman operator*

$$(\mathcal{T}_{\text{rob}}V)(s) := \max_{a \in \mathcal{A}(s)} \min_{P(\cdot|s,a) \in U_{s,a}} \left\{ r(s, a) + \gamma \mathbb{E}_P[V(S')] \right\} \quad (20)$$

is a  $\gamma$ -contraction on  $(\mathbb{R}^{|S'|}, \|\cdot\|_\infty)$  with modulus  $\gamma$ , where

$$\mathbb{E}_P[V(S')] = \sum_{s' \in S'} P(s' | s, a) V(s'). \quad (21)$$

**Assumption 3** (Posterior and credible sets). *The Bayesian posterior  $p(\theta_v | \mathcal{D}_t)$  is well defined on a compact parameter space  $\Theta$ , where  $\mathcal{D}_t$  denotes all data observed up to time  $t$ . For each node  $v$ , the credible set  $U_v^t \subseteq \Theta$  is Borel measurable.<sup>1</sup>*

**Assumption 4** (Posterior tightness and eventual nesting). *For each  $v$ , there exists a target threat type  $\theta_v^* \in \Theta$  such that  $\mathbb{P}(\theta_v^* \in U_v^t) \rightarrow 1$  and  $\sup_{\theta, \theta' \in U_v^t} \|\theta - \theta'\|_\infty \rightarrow 0$  in probability as  $t \rightarrow \infty$ , where  $\|\cdot\|_\infty$  denotes the sup-norm on the threat parameter space  $\Theta$ . There exists a random finite time after which  $U_v^{t+1} \subseteq U_v^t$  holds for all  $t$ .*

**Assumption 5** (Stepwise continuity and dominated convergence). *For any  $(v, a)$ , the maps  $\theta \mapsto \mathbb{E}_{P(o|a, \theta)}[o]$  and  $\theta \mapsto p_{\text{exp}}(a, \theta)$  are continuous on  $\Theta$ . If the observation space is infinite, there exists an integrable dominating function  $g(o)$  such that  $\sup_{\theta \in \Theta} |\varphi(o)| \leq g(o)$  and  $\int_{\mathcal{O}} g(o) \mu(\text{d}o) < \infty$ , so that dominated convergence applies. Hence, for compact  $U \subseteq \Theta$ , the map  $U \mapsto \min_{\theta \in U} f_{v,a}(\theta)$  is continuous under set convergence in Painlevé–Kuratowski (PK) sense.<sup>2</sup>*

**Assumption 6** (Greedy selection and tie-breaking). *Action sets  $\mathcal{A}(s)$  are finite for all  $s$ . A measurable tie-breaking rule (i.e., a tie-breaker that defines a Borel-measurable action mapping) is fixed. If the optimal action is unique for each state under the true parameter  $\theta^*$ , then the greedy selector will pick a single, well-defined action in the limit.*

These assumptions jointly ensure that the robust Bellman operator is well-defined, contractive, and stable under learning. Discounting turns the infinite-horizon objective into a convergent power series and bounds the influence of remote outcomes, while uniform boundedness ensures that the Bellman update remains within a compact set. Bounded one-stage rewards imply that any fixed point satisfies  $\|V\|_\infty \leq R_{\max}/(1 - \gamma)$ , where  $R_{\max} := \sup_{s,a} |r(s, a)|$ . This uniform ensures  $V_t$  remains in the closed ball of  $(\mathbb{R}^{|S'|}, \|\cdot\|_\infty)$  and allows Banach’s fixed-point theorem<sup>3</sup> to apply without additional growth conditions. If these assumptions are violated, for example, when  $\gamma \geq 1$  or the rewards are unbounded, value iteration may diverge or fail to admit a finite fixed point. Even if a policy is mathematically well defined, small modeling errors can accumulate and undermine safety guarantees. In most engineered systems, physical

<sup>1</sup>A set is Borel measurable if it lies in the Borel  $\sigma$ -algebra  $\mathcal{B}(\Theta)$ , the smallest  $\sigma$ -algebra containing all open subsets of  $\Theta$ . This ensures that probabilities and expectations with respect to measures on  $\Theta$  are well defined.

<sup>2</sup>Formally, PK convergence is defined through the convergence of inner and outer limits of sets [44]. In this framework,  $U_v^t \rightarrow \{\theta_v^*\}$  means that every sequence  $\theta_t \in U_v^t$  has limit points contained in  $\{\theta_v^*\}$  and that the true parameter  $\theta_v^*$  can be approximated by points from  $U_v^t$  for all large  $t$ .

<sup>3</sup>Let  $(X, d)$  be a complete metric space and let  $T : X \rightarrow X$  be a contraction. There exists  $\gamma \in (0, 1)$  such that  $d(Tx, Ty) \leq \gamma d(x, y)$  for all  $x, y \in X$ . Then  $T$  admits a unique fixed point  $x^* \in X$ , and the iterates  $T^t x_0$  converge to  $x^*$  for any initial point  $x_0 \in X$  [45].

limits or budget caps impose natural bounds. We ensure that any additional penalty terms remain bounded so that the uniform bound on the value function remains valid.

Rectangularity decouples ambiguity across state–action pairs, which removes adversarial coupling effects across time. This decoupling is exactly what makes the inner minimization separable and ensures the Bellman recursion holds in the presence of uncertainty over the transition probabilities. Contraction with modulus  $\gamma$  ensures uniqueness of the robust value and geometric error decay for value iteration and policy evaluation. Without contraction, limit points may not exist, and set-valued Bellman maps can exhibit cycling, highlighting the role of boundedness and discounting. Rectangularity is a simplifying but conservative assumption: it ignores correlations between transitions of different  $(s, a)$  pairs, making the problem more tractable but potentially less tight.

Compact credible sets and measurability ensure that Bayesian learning can be embedded in the planning process. Compactness ensures that the posterior remains confined to a bounded region of the parameter space, which is essential for establishing uniform continuity. Measurability ensures that the data-driven sets can be embedded into the filtration, a family of time-indexed  $\sigma$ -algebras encoding the information revealed up to time  $t$ , so that the operators are random but well-defined. Compactness of the parameter space  $\Theta$  and the credible set  $U_v^t$  being Borel measurable guarantee existence of minimizers when taking  $\min_{\theta \in U_v^t}$  and enable measurable selection for greedy policies and inner minimizers, meaning that the resulting selectors are Borel-measurable functions of the state. These properties are used implicitly to justify interchanging max, min, and expectations.

Posterior tightness captures the idea that uncertainty shrinks as learning progresses. When each credible set only shrinks over time, the corresponding Bellman operators stop oscillating and approach a stable limit. Together, they imply that the algorithm eventually uses the Bellman operator corresponding to the true parameter. Tightness means that each credible set converges to the true parameter in PK sense. This is what underpins operator convergence in Corollary 1. Eventual nesting allows monotonicity arguments that simplify the proof of almost sure convergence of the fixed points. If credible sets expand intermittently due to model misspecification, the derived safety bounds no longer provided useful protection. If sets shrink to the wrong point with positive probability, the limit policy can be biased.

Continuity ensures that small changes in posterior beliefs produce only small adjustments in the chosen action or value, preventing discontinuous control switches as uncertainty decreases. Dominated convergence is the technical bridge that lets limits pass through expectations, which is essential because the Bellman operator computes an expectation with respect to transition probabilities that depend on the parameter. With domination,<sup>4</sup> we have that  $\lim_{t \rightarrow \infty} \mathbb{E}_P[\varphi_t(o)] = \mathbb{E}_P[\lim_{t \rightarrow \infty} \varphi_t(o)]$ , which is used to show continuity of the inner minima with respect to set limits. This is what yields uniform convergence of operators on bounded sets. In our setting, the parameter space  $\Theta$  is discrete, so both conditions hold automatically. Every map  $\theta \mapsto f_{v,a}(\theta)$  is continuous, and expectations reduce

<sup>4</sup>By dominated convergence, pointwise convergence of  $\{\varphi_t\}$  together with an integrable dominating envelope  $g$  allows the limit to pass through the expectation with respect to the parameterized probability measures under the standard conditions of dominated convergence [46].

to finite sums, making dominated convergence trivially valid. We retain this assumption for generality, so that the same theoretical statements extend without modification to continuous parameter spaces or models with continuous observations.

Finite action sets and a fixed tie-breaking rule prevent policy instability. The algorithm repeatedly selects greedy actions from a possibly set-valued argmax. A fixed rule avoids random policy fluctuations that would confound convergence and policy limit arguments. Finiteness makes the argmax operator upper hemicontinuous<sup>5</sup> with nonempty, compact values. A measurable selector then exists, i.e., a Borel-measurable state-to-action function chosen from each argmax set. Uniqueness in the limit upgrades set convergence of  $Q$ -values to pointwise convergence of deterministic policies.

## 2. Operator Convergence under Shrinking Ambiguity Sets

As the ambiguity sets evolve with data, the robust Bellman operator itself changes over time. A key question is whether value iteration driven by these data-dependent operators remains convergent and stable. The assumptions above ensure boundedness and a common  $\gamma$ -contraction modulus; thus, the operators approach a limiting operator uniformly on bounded subsets. The next theorem formalizes this convergence and shows that the iterates follow the limiting operator almost surely.

**Theorem 1** (Almost sure convergence of the adaptive robust value iteration). *Let  $(\Omega, \mathcal{F}, \mathbb{P})$  be a probability space and  $\{\mathcal{F}_t\}_{t \geq 0}$  an increasing filtration.<sup>6</sup> Let  $\{\mathcal{T}_{\text{rob}}^t\}_{t \geq 0}$  be a sequence of random robust Bellman operators, each  $\mathcal{F}_t$ -measurable, induced by random ambiguity sets  $\{U_{s,a}^t\}_{(s,a)}$  that are  $\mathcal{F}_t$ -measurable. Suppose Assumptions 1–6 hold and that, almost surely, for every bounded set  $B \subset \mathcal{B}$  with  $\mathcal{B} := \{V : \mathcal{S}' \rightarrow \mathbb{R} \text{ bounded}\}$ ,*

$$\sup_{V \in B} \|\mathcal{T}_{\text{rob}}^t(\omega)V - \mathcal{T}_{\infty}(\omega)V\|_{\infty} \longrightarrow 0, \text{ for } \mathbb{P}\text{-almost every } \omega \in \Omega, \quad (22)$$

where  $\mathcal{T}_{\infty}(\omega)$  denotes the operator obtained as  $t \rightarrow \infty$ . Since each  $\mathcal{T}_{\text{rob}}^t(\omega)$  is a  $\gamma$ -contraction with common modulus,  $\mathcal{T}_{\infty}(\omega)$  is also a  $\gamma$ -contraction on  $(\mathcal{B}, \|\cdot\|_{\infty})$ . Then there exists  $\Omega_0 \subseteq \Omega$  with  $\mathbb{P}(\Omega_0) = 1$  such that, for every  $\omega \in \Omega_0$ , the value iteration

$$V_{t+1}(\omega) = \mathcal{T}_{\text{rob}}^t(\omega)V_t(\omega) \quad (23)$$

converges to the unique fixed point  $V^*(\omega)$  of  $\mathcal{T}_{\infty}(\omega)$ , i.e.,  $V_t(\omega) \rightarrow V^*(\omega)$  with  $\mathcal{T}_{\infty}(\omega)V^*(\omega) = V^*(\omega)$ .

*Proof.* See Appendix A. □

<sup>5</sup>A set-valued map  $F : X \rightrightarrows Y$  assigns to each  $x \in X$  a subset  $F(x) \subseteq Y$ . It is upper hemicontinuous at  $x$  if for every open set  $O$  containing  $F(x)$ , there exists a neighborhood  $N$  of  $x$  such that  $F(x') \subseteq O$  for all  $x' \in N$ . Intuitively, it means that the graph of  $F$  does not jump upward in the limit, so the possible argmax sets vary continuously under small perturbations [44].

<sup>6</sup>A filtration  $\{\mathcal{F}_t\}$  is an increasing sequence of  $\sigma$ -algebras representing the information available up to time  $t$ . A random variable or operator is  $\mathcal{F}_t$ -measurable if it depends only on data observed up to time  $t$ .

**Remark 1** (Interpretation and application of Theorem 1). *Theorem 1 refines pointwise, data-driven operator convergence to convergence of the computed values along the actual iteration run by the algorithm. The result guarantees that the algorithm converges almost surely for the observed data sequence. Uniform convergence on bounded sets ensures that the operator behaves consistently, regardless of the current iterate. A common modulus of contraction ensures that the limiting operator still satisfies the same  $\gamma$ -contraction property. Losing contraction leads to instability and the potential absence of a fixed point, so maintaining a uniform modulus is essential.*

Since value iteration converges to the fixed point of the limiting operator, the algorithm behaves as if the transition model were fixed once the credible sets stabilize. When they collapse to the true parameters, the limiting operator becomes the nominal Bellman operator. The following corollary formalizes this.

**Corollary 1** (Asymptotic optimality). *Under Assumptions 1–6, suppose that  $U_v^t \rightarrow \{\theta_v^*\}$  almost surely for all  $v$ . Define  $U_{s,a}^t = \phi_{s,a}(U_{v(s,a)}^t)$  and  $U_{s,a}^\infty := \{\phi_{s,a}(\theta_{v(s,a)}^*)\}$ . Then,  $\mathcal{T}_{\text{rob}}^t \rightarrow \mathcal{T}_{\text{nom}}^{\theta^*}$  almost surely, uniformly on bounded subsets of  $\mathcal{B}$ , where*

$$(\mathcal{T}_{\text{nom}}^{\theta^*} V)(s) = \max_{a \in \mathcal{A}(s)} \left\{ r(s, a) + \gamma \mathbb{E}_{P^*(\cdot|s,a)} [V(S')] \right\}. \quad (24)$$

*By Theorem 1,  $V_t \rightarrow V_{\text{nom}}^*$  almost surely. If, in addition, the optimal action is unique at every state for the limit operator, then the greedy policies  $\pi_t$  converge almost surely to the nominal optimal policy  $\pi_{\text{nom}}^*$ . Without uniqueness, any sequence of greedy policies admits convergent subsequences whose limits are optimal.*

**Remark 2** (Operational meaning of asymptotic optimality). *As the credible sets contract to the true parameter, the uncertainty in the transition kernel disappears, and the robust formulation converges to the planning problem defined by the true model. The algorithm therefore transitions from conservative exploration to exploitation and ends up computing exactly the nominal optimal policy. Uniformity on bounded sets is needed to interchange limits with the outer maximization and to avoid dependence on the particular trajectory of  $V_t$ . This is what converts operator convergence into value convergence along the value sequence generated by the algorithm. Uniqueness gives pointwise convergence of policies. When multiple actions are optimal, the result still guarantees that any limit point is optimal.*

### 3. Safety and Computational Properties

While asymptotic optimality characterizes the long-run behavior of the adaptive planner, safety concerns arise during learning: the model is uncertain, and policies are selected based on ambiguity sets rather than the true transition kernel. A natural question is whether the robust value used for planning provides conservative guarantees on realized performance under the true dynamics. The next proposition shows that Assumption 2 yields such probabilistic safety guarantees.

**Proposition 1** (Probabilistic safety guarantee under  $(s, a)$ -rectangular uncertainty). *Let  $(\Omega, \mathcal{F}, \mathbb{P})$  be a probability space and  $\{\mathcal{F}_t\}$  a filtration, i.e., an increasing family of  $\sigma$ -algebras representing the information available up to time*

$t$ . For each node  $v$ , let  $U_v^t \subseteq \Theta$  be an  $\mathcal{F}_t$ -measurable Borel set. Assume the following structural conditions. There is a partition of state–action pairs induced by a mapping  $v : \mathcal{S} \times \mathcal{A} \rightarrow \mathcal{V}$ , where  $v(s, a)$  denotes the node to which the pair  $(s, a)$  belongs, and Borel measurable maps

$$P(\cdot \mid s, a; \theta) := \phi_{s,a}(\theta_{v(s,a)}), \quad \phi_{s,a} : \Theta_{v(s,a)} \rightarrow \Delta(\mathcal{S}'). \quad (25)$$

Define the  $(s, a)$ -marginal ambiguity sets by

$$U_{s,a}^t := \phi_{s,a}(U_{v(s,a)}^t) \subseteq \Delta(\mathcal{S}'), \quad (26)$$

and the rectangular ambiguity set

$$U^t := \prod_{(s,a)} U_{s,a}^t \subseteq \prod_{(s,a)} \Delta(\mathcal{S}'). \quad (27)$$

where  $\prod$  denotes the Cartesian product over sets. Each  $U_v^t$  is nonempty and compact by Assumption 3. Each  $\phi_{s,a}$  is continuous by Assumption 5. Hence  $U_{s,a}^t$  is nonempty and compact, and  $U^t$  is nonempty and compact. Let the credible event be

$$\mathcal{E}_t := \{\theta_v^* \in U_v^t \text{ for all } v\}, \quad (28)$$

and let  $P^*$  be the true transition model generated by the true local parameters, that is,  $P^*(\cdot \mid s, a) = \phi_{s,a}(\theta_{v(s,a)}^*)$ . Let  $\pi_t$  be any stationary policy greedy with respect to the robust value under rectangular ambiguity set  $U^t = \prod_{(s,a)} U_{s,a}^t$ . Then

$$\mathbb{P}\left(\forall s \in \mathcal{S}' : V_{P^*}^{\pi_t}(s) \geq \min_{P \in U^t} V_P^{\pi_t}(s)\right) \geq 1 - \delta_t, \quad \delta_t := \mathbb{P}(\mathcal{E}_t^c). \quad (29)$$

Here,  $\delta_t$  is the probability that the true parameter lies outside the credible sets, so with probability  $1 - \delta_t$  the ambiguity sets contain the true model and the robust value lower bound holds for all states in  $\mathcal{S}'$ .

*Proof.* See Appendix A. □

**Remark 3** (Safety guaranteed by the robust value). *Conditioned on the event that the true parameters lie in the credible sets, the realized value under the true kernel dominates the worst-case value used for planning. In other words, the planner’s predicted robust value is a conservative lower bound on its actual performance. The shortfall term  $\delta_t$  is the probability that the credible set does not include the true parameter at time  $t$ . Improving statistical coverage is the primary lever to tighten the guarantee. Under  $(s, a)$ -rectangularity, the inner minimization is exact on each local transition model, so the robust planner already evaluates the worst-case model without approximation. The result holds uniformly with respect to the state and for any greedy policy with respect to the robust value, so it applies to both evaluation and improvement steps.*

Beyond safety, it is important to understand the computational cost of implementing the adaptive robust planner. Each replan operates with a fixed family of credible sets and performs robust value iteration until convergence. The following proposition provides a per-replan complexity bound and clarifies how the uncertainty size affects the computational cost.

**Proposition 2** (Per-replan complexity). *During each replan, the family of credible sets  $\{U_v^t\}$  are fixed, and robust value iteration is performed until the value updates are within a tolerance  $\varepsilon$ . Since the Bellman operator is a  $\gamma$ -contraction, the value iteration requires  $N_\varepsilon = O(\log(1/\varepsilon)/(1-\gamma))$  iterations to ensure that the value updates are within tolerance  $\varepsilon$ . Each robust reward  $\tilde{r}_{\text{rob}}(v, a, U_v^t)$  can be evaluated in  $O(|\overline{U^t}|)$  time using precomputed expectations, where  $|\overline{U^t}|$  is the average ambiguity set size across nodes. Then, the per-replan computational cost is*

$$O\left(N_\varepsilon (|S'| |\overline{\mathcal{A}}| + |S| |\mathcal{A}_S| |\overline{U^t}|)\right), \quad (30)$$

where  $|\overline{\mathcal{A}}|$  is the average number of actions per state.

*Proof.* See Appendix A. □

**Remark 4** (Interpretation of complexity). *The two terms reflect distinct computations within each replan: the first term accounts for Bellman updates over state space  $S'$ , and the second term for robust evaluations within ambiguity sets. Together, the two terms represent the total per-replan workload. As learning progresses and uncertainty about the parameters decreases, the algorithm needs to evaluate fewer models within each ambiguity set. Consequently, the expected computational cost per replan gradually approaches the standard value iteration under the true model.*

## VII. Results

We conduct three numerical experiments under different environmental and structural conditions to validate the proposed adaptive robust planner. Experiment 1 tests whether the planner operates as intended and converges in a controlled environment with Gaussian threat models. Experiment 2 tests robustness and generalization to non-Gaussian threat models, including Gaussian mixtures and log-normal distributions. Experiment 3 evaluates the scalability and consistency of the planner as the network topology and size vary.

### A. Baseline Implementations

To evaluate the performance of the proposed adaptive robust planner, we compare it against two baselines: *static robust* and *nominal* planning. These baselines are two complementary extremes in terms of uncertainty handling and adaptability. Both baselines share the same sensing–movement structure and update routines as Algorithm 1, but differ in how they treat and propagate uncertainty during planning.

In the static robust baseline, the ambiguity sets of possible threat types remain fixed throughout the entire mission. The logic of the static robust planner is summarized in Algorithm 2. It optimizes actions through a minmax value-iteration process that selects the best decision under the worst-case threat configuration within each static set. As a result, it provides strong safety guarantees but is often overly conservative. Since the uncertainty representation is never refined, the planner tends to overestimate risk and produce cautious but suboptimal behavior.

---

**Algorithm 2** Static Robust Planning

---

```

1: Initialize fixed parameter sets  $\bar{U}_v \subseteq \Theta$  for all  $v$  and the ambiguity set is induced as  $U_{s,a} = \phi_{s,a}(\bar{U}_v)$ .
2: for  $t = 0, 1, \dots, T - 1$  do
3:   for each sense action  $a \in \mathcal{A}_{S'}$  do
4:     Compute static robust surrogate:  $\tilde{r}_t(v, a) = \min_{P \in U_{s,a}} \left[ \mathbb{E}_{P(o|a)}[o] + \lambda_{\text{imm}}(-p_{\text{exp}}(a, P)) \right] - c_{\text{sense}}(a)$ 
5:   end for
6:   Choose action:  $a_t = \arg \max_{a \in \mathcal{A}_{S'}} \{ \tilde{r}_t(v_t, a) + \lambda_{\text{nov}} n_t(v) + \gamma V(v_t, M') \}$ 
7: end for

```

---

The nominal baseline uses the maximum *a posteriori* (MAP) principle to address uncertainty. The overall procedure of the nominal planner is outlined in Algorithm 3. After each observation, the planner infers the most probable threat type at each node based on the current posterior belief. The planner then selects the next actions, assuming those estimates are correct. This approach reflects an optimistic decision-making strategy that commits to the maximum-probability threat hypothesis under the current posterior. It enables efficient and confident decisions when the belief model is accurate. However, it can become overconfident and fragile in highly uncertain or noisy environments.

---

**Algorithm 3** Nominal Planning

---

```

1: Initialize belief  $b_{0,v}(\theta) = 1/|\Theta|$  for all  $v \in \mathcal{S}$ 
2: for  $t = 0, 1, \dots, T - 1$  do
3:   Observe signal  $o_t$  at current node  $v_t$ 
4:   Update belief via Bayes rule:  $b_{t+1,v_t}(\theta) = \frac{b_{t,v_t}(\theta) p(o_t | a_t, \theta)}{\sum_{\theta' \in \Theta} b_{t,v_t}(\theta') p(o_t | a_t, \theta')}$ 
5:   Compute MAP estimate:  $\hat{\theta}_{v_t} = \arg \max_{\theta} b_{t+1,v_t}(\theta)$ 
6:   for each sense action  $a \in \mathcal{A}_{S'}$  do
7:     Compute nominal surrogate:  $\tilde{r}_t(v_t, a) = \mathbb{E}_{P(o|a,\hat{\theta}_{v_t})}[o] + \lambda_{\text{imm}}(-p_{\text{exp}}(a, \hat{\theta}_{v_t})) - c_{\text{sense}}(a)$ 
8:   end for
9:   Choose action:  $a_t = \arg \max_{a \in \mathcal{A}_{S'}} \{ \tilde{r}_t(v_t, a) + \lambda_{\text{nov}} n_t(v) + \gamma V(v_t, M') \}$ 
10: end for

```

---

## B. Experiment 1: Basic Validation in a Controlled Environment

This experiment verifies that the proposed adaptive robust planner operates as intended in a simplified and well-controlled setting. We consider a small grid network in which each threat type induces Gaussian observation and exposure models, allowing us to confirm that the planner converges to stable policies, correctly updates its ambiguity sets, and reproduces the expected behavior under idealized conditions. This setting conceptually reflects controlled ISR mission test ranges where conditions are intentionally idealized [47], providing a clean environment for baseline

validation before moving to larger and more uncertain scenarios.

The environment is configured as a  $3 \times 4$  grid graph consisting of 12 nodes. Each node is assigned one of three latent threat types, denoted as  $\theta \in \{1, 2, 3\}$ . The agent can choose among four sensing actions  $a \in \{A, B, C, D\}$ , each producing an observation  $o \sim \mathcal{N}(\mu_{a,\theta}, \sigma_{a,\theta})$  and an associated exposure score that determines exposure risk. Exposure follows a Gaussian model with mean  $\mu_{a,\theta}^{\text{haz}}$  and standard deviation  $\sigma_{a,\theta}^{\text{haz}}$ ; an exposure event occurs when the score exceeds a threshold of 0.5, chosen as a neutral cutoff for the experiment. The immediate sensing reward combines the observation value, sensing cost, and exposure penalty, while movements between neighboring nodes incur a fixed cost. A discount factor  $\gamma = 0.98$  and additional penalty components model persistent and cumulative exposure effects. The key simulation parameters are summarized in Table 3.

**Table 3 Key simulation parameters for Experiments 1**

| Parameter                  | Description  | Value / Setting          |
|----------------------------|--|--------------------------|
| Threat types               | $\theta \in \{1, 2, 3\}$   | 3 categories             |
| Sensing actions            | $a \in \{A, B, C, D\}$   | 4 actions                |
| Observation model          | $o \sim \mathcal{N}(\mu_{a,\theta}, \sigma_{a,\theta})$                                    | Gaussian                 |
| Exposure model             | $\eta_{v,t} \sim \mathcal{N}(\mu_{a,\theta}^{\text{haz}}, \sigma_{a,\theta}^{\text{haz}})$ | Gaussian                 |
| Exposure threshold         | $\tau_\eta$  | 0.5                      |
| Discount factor            | $\gamma$   | 0.98                     |
| Movement cost              | $c_{\text{move}}$  | 1.0                      |
| Sensing cost               | $c_{\text{sense}}(a)$  | $\{1.0, 1.0, 1.0, 0.1\}$ |
| Immediate exposure weight  | $\lambda_{\text{imm}}$   | 50.0                     |
| Persistent decay rate      | $\alpha$   | 0.95                     |
| Persistent exposure weight | $\lambda_{\text{pers}}$  | 0.1                      |
| Cumulative exposure weight | $\lambda_{\text{cum}}$   | 0.0005                   |
| Novelty weight             | $\lambda_{\text{nov}}$   | 1                        |
| Novelty decay rate         | $\beta$  | 0.8                      |
| Replan frequency           | $k$ (steps per replan)   | 1                        |

We compare the adaptive robust planner against the static robust and nominal baselines under identical settings. Each planner operates for up to 2000 time steps, replanning at every step ( $k = 1$ ). Performance is evaluated based on three key metrics: (i) the average observation reward and cumulative reward over time, (ii) the convergence behavior of the average credible set size  $|U_v^t|$  (for the adaptive robust planner only), and (iii) exposure statistics that capture both persistent and cumulative penalty effects. These metrics collectively illustrate how the planner balances reward maximization and risk mitigation as it progressively refines its uncertainty representation.

All experiments use fixed random seeds for graph generation and threat initialization to ensure reproducibility while maintaining stochastic observation and exposure outcomes. Before presenting quantitative results, we visualize the underlying reward and hazard structures to clarify how the planner perceives the trade-off between sensing benefit and exposure risk in Figures 4 and 5. The sensing actions A through D correspond to the four available sensing modes defined in the threat–observation model. As shown, each threat type favors a distinct action that simultaneously enables



more advantageous decisions. Action D, in contrast, serves as a safer default option when little information about the true threat type is available. Movement actions allow the aircraft to transition to adjacent nodes in the graph, but they are not depicted here since the figures focus solely on sensing-related reward and hazard patterns.

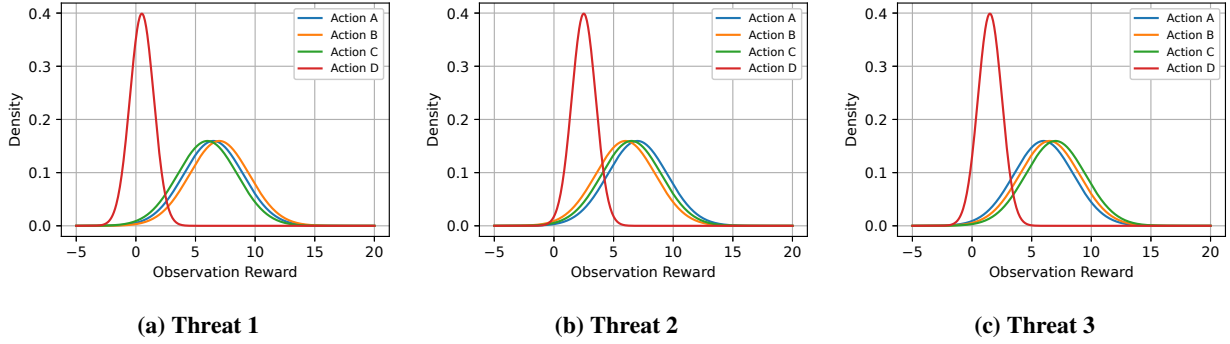


**Fig. 4** Comparison of reward distributions across different threat prototypes for Experiment 1. Each subplot shows the probability density of expected observation rewards for all available actions under a specific threat.

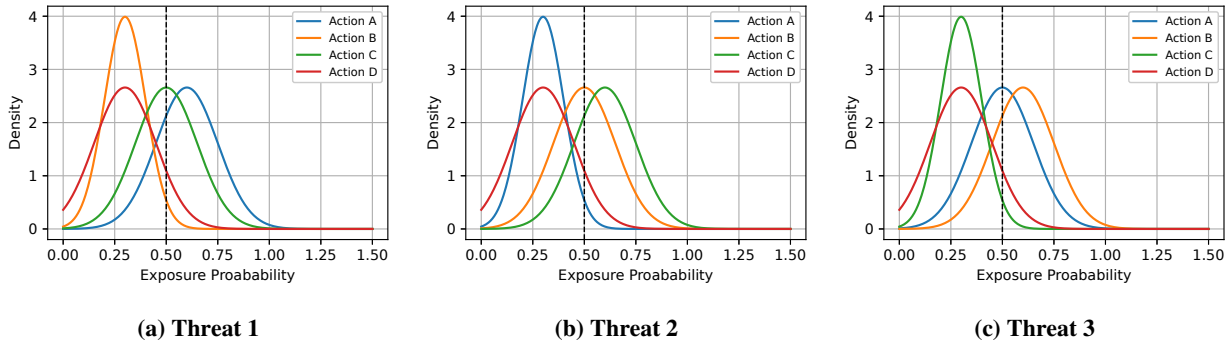


**Fig. 5** Exposure probability distributions corresponding to the threat prototypes in Experiment 1. The dashed vertical line indicates the decision threshold. Samples with exposure probability greater than 0.5 are considered exposed under the corresponding threat condition.

**Table 4** Summary of Experiment 1 Results. Higher values are better for observation and total reward, while lower values are better for cumulative exposures.

| Planner         | Observation Reward $\uparrow$          | Cumulative Exposures $\downarrow$   | Total Reward $\uparrow$                 |
|-----------------|--|-------------------------------------|---|
| Adaptive Robust | $5882.44 \pm 168.12$                   | <b><math>39.13 \pm 11.19</math></b> | <b><math>9861.38 \pm 1345.84</math></b> |
| Nominal         | <b><math>6780.49 \pm 108.32</math></b> | $240.92 \pm 65.92$                  | $-7782.01 \pm 4887.74$                  |
| Static Robust   | $1487.82 \pm 233.79$                   | $89.64 \pm 9.16$                    | $190.63 \pm 858.26$                     |

Table 4 presents the results of Experiment 1, where each value is listed as mean  $\pm$  standard deviation across 100 runs. The three planners display clearly different behaviors. The adaptive robust planner performs best overall, achieving high total rewards while keeping the number of exposures low. This means it learns to gather useful information without taking excessive risks. As its belief about threats becomes more confident, the policy naturally shifts from

cautious exploration to more efficient sensing and movement. The nominal planner, which assumes a single estimated threat model, gains higher observation rewards early on but suffers from heavy exposure penalties and unstable total returns. Its aggressive sensing leads to frequent exposures, showing that overconfidence under uncertainty can reduce mission survivability. The static robust planner takes the opposite approach: it keeps the ambiguity sets fixed, acts conservatively to avoid risk, but gathers little information and achieves low overall rewards. Together, these results demonstrate that the adaptive robust planner provides the best balance between safety and efficiency. It remains robust when uncertainty is high and approaches nominal-level performance as threat ambiguity at each node decreases.

Additionally, we also evaluated the computational efficiency of each planner to assess online feasibility. All experiments were conducted on a standard CPU node of the University of Michigan Great Lakes computing cluster, equipped with dual Intel Xeon Gold 6154 processors (36 cores, 3.0 GHz) and 187 GB RAM. Each run used 4 CPU cores and 8 GB of memory without GPU acceleration. For the 2000-step simulations in Experiment 1, the nominal planner required an average of  $43.46 \pm 0.07$  s (approximately 21.7 ms per step), the adaptive robust planner  $63.82 \pm 0.47$  s (31.9 ms per step), and the static robust planner  $94.14 \pm 0.34$  s (47.1 ms per step). All planners operated fast enough for online execution, with each decision step completed within tens of milliseconds. Notably, the adaptive robust planner ran faster than the static robust planner because it gradually narrowed the ambiguity set during execution. As the planner refined its uncertainty over time, the computations became simpler while still supporting real-time operation.

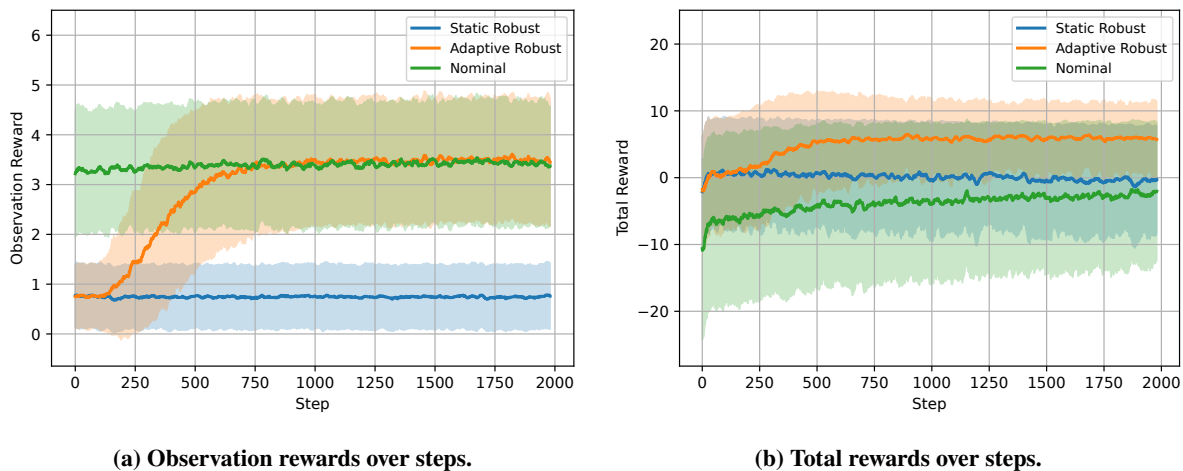


**Fig. 6 Results of Experiment 1 comparing the reward evolution across three planning strategies. Both plots show 20-step moving-averaged results across random seeds. (a) Step-wise observation rewards. (b) Step-wise total rewards, including exposure penalties. Solid lines indicate the averaged performance across random seeds, and the shaded regions represent  $\pm 1$  standard deviation.**

Figure 6 presents how each planner’s rewards evolve over time. The observation rewards are shown in Figure 6a. Initially, the nominal planner earns higher rewards because of its optimistic decision-making approach. In contrast, both the adaptive robust and static robust planners begin with lower values due to their conservative strategies under ambiguity sets. Over time, the static robust planner maintains nearly constant rewards because its fixed ambiguity set

leads to repetitive behavior under similar conditions. Conversely, the adaptive robust planner gradually shrinks its ambiguity set, increasing observation rewards that approach those achieved by the nominal planner. The observation rewards increase smoothly as each node in the graph maintains its own ambiguity set. Some nodes quickly identify one threat prototype as most likely, whereas others remain ambiguous and continue to consider several possible threat types.

Figure 6b illustrates the evolution of total rewards, which incorporate exposure penalties. The adaptive robust planner consistently achieves the best performance among the three approaches. Although the nominal planner secures higher observation rewards, its exposure risk reduces its total gains. Despite gradual improvement through ongoing belief updates and MAP estimation, the nominal planner exhibits a wider standard deviation band, reflecting unstable performance. In contrast, the adaptive robust planner initially performs similarly to the static robust planner but soon improves as its ambiguity set contracts, achieving high, stable total rewards. Since the static robust planner maintains a larger ambiguity set than the adaptive robust planner at all times, it serves as a lower bound on performance under uncertainty.

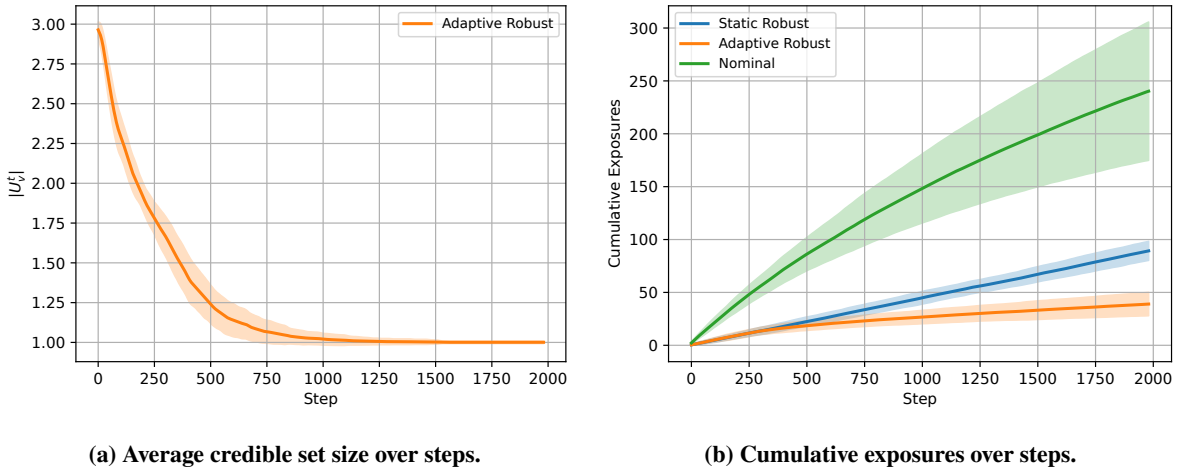
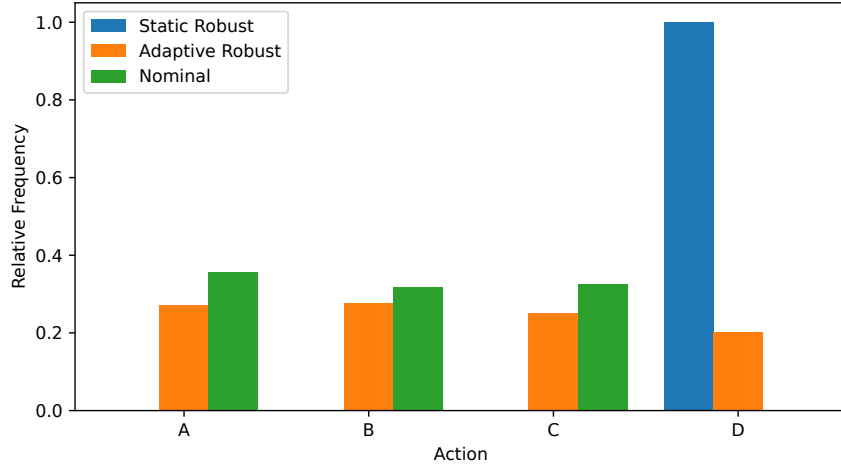


**Fig. 7 Results of Experiment 1. (a) Step-wise changes in the credible set size  $|U_v^t|$  for the adaptive robust planner, illustrating how uncertainty is reduced over time. (b) Cumulative number of exposures over steps, compared across the three planning strategies. Both plots present 20-step moving-averaged results across random seeds. The solid lines denote the mean, and the shaded regions represent one standard deviation.**

Figure 7 illustrates how each planner behaves within the simulation environment beyond the reward metrics. Figure 7a shows the evolution of the average credible set size of the adaptive robust planner across all graph nodes over time. From step 0 to approximately 500, the credible set size decreases sharply, indicating a rapid reduction in uncertainty. Beyond this point, the curve flattens as the planner revisits a few nodes that remain difficult to classify. Eventually, the credible set size converges to 1 for all nodes, indicating that the threats associated with each node are correctly identified.

Figure 7b presents the cumulative exposures over time. The nominal planner exhibits a notably higher exposure

rate than the others due to the optimistic policy. The adaptive robust and static robust planners perform similarly up to around step 500. After that, the adaptive robust planner shows lower exposure rates. This trend occurs because our experimental setup rewards planners which accurately identify each node’s threat, giving them an advantage as uncertainty decreases. Notably, the stepwise total reward can exceed the observation reward, as it includes a novelty term that provides a positive exploration bonus for visiting less-explored nodes. Together, these results demonstrate that the adaptive robust planner maintains robustness in uncertain environments while naturally improving efficiency, thereby achieving the intended balance between the two.



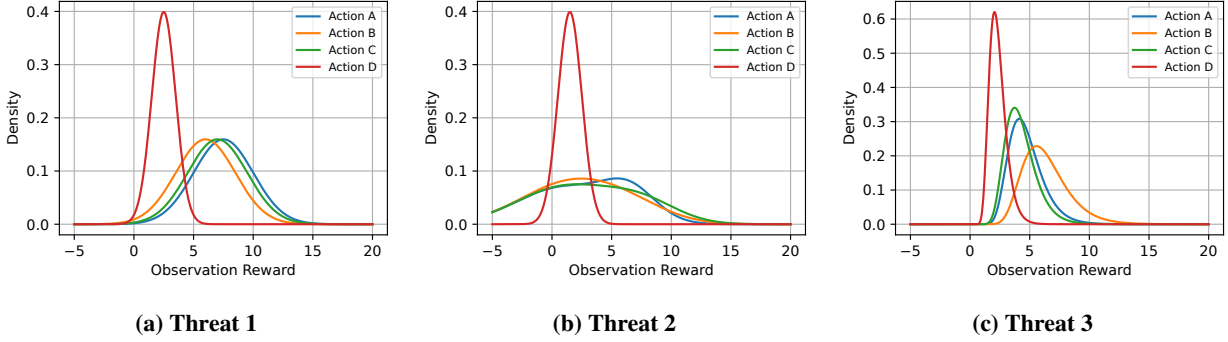
**Fig. 8 Distribution of sensing action selections across different policies in Experiment 1. Action labels (A–D) correspond to the mapped sense-action categories. Frequencies are normalized to show relative selection ratios.**

Figure 8 illustrates how each planner selected sensing actions in Experiment 1, clearly revealing their distinct decision-making strategies. The static robust planner consistently chooses only action D, the safest option when the threat type is uncertain. This conservative behavior results in relatively low observation and total rewards. In contrast, the nominal planner, which relies on the MAP estimate, avoids action D and selects actions A, B, and C depending on its belief about each node’s threat type. The adaptive robust planner combined the strengths of both approaches, showing a balanced distribution across all four actions (A–D). It initially behaved conservatively, like the static robust planner, but gradually shifted toward higher-reward actions as the threat type became more certain.

### C. Experiment 2: Generalization to Non-Gaussian Threat Models

We assess the planner’s robustness and adaptability under general threat models, including Gaussian mixtures and log-normal distributions. These distributions capture multimodal and heavy-tailed sensing patterns commonly observed in electronic warfare environments [48], allowing us to test whether the planner generalizes beyond the idealized Gaussian assumptions of Experiment 1. The modified experimental parameters are summarized in Table 5. With the same 3×4 grid graph and the same action set as in Experiment 1, we modify the observation and exposure models to

capture more diverse threat prototypes. The reward and exposure models used in Experiment 2 for all three threats are shown in Figures 9 and 10. Specifically, Threats 1 and 2 use Gaussian mixture observation models, where a single Gaussian is treated as a special (degenerate) case, while Threat 3 adopts a log-normal observation model. Each run consists of 3000 planning steps and is simulated under 100 independent random seeds. We evaluate whether the adaptive robust planner remains effective under non-Gaussian uncertainty, exhibiting similar patterns in ambiguity refinement and exposure management to those observed in Experiment 1.



**Fig. 9** Comparison of reward distributions across different threat prototypes for Experiment 2. Each subplot shows the probability density of expected observation rewards for all available actions under a specific threat.

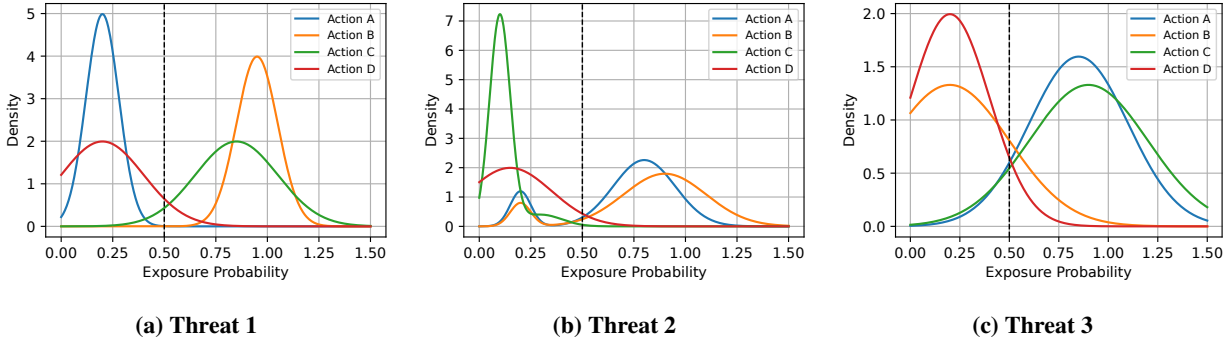


**Fig. 10** Exposure probability distributions corresponding to the same threat prototypes in Experiment 2. The dashed vertical line indicates the decision threshold. Samples with exposure probability greater than 0.5 are considered exposed under the corresponding threat condition.

Table 6 summarizes the quantitative results obtained under modified threat models. Despite the changes in both the observation and exposure distributions, the overall performance trend remains consistent with that observed in Experiment 1. The adaptive robust planner continues to achieve substantially higher total rewards compared to the nominal and static robust baselines, while continuing to keep cumulative exposures low. This consistency indicates that the proposed adaptive robust approach remains effective beyond Gaussian threat assumptions, generalizing across broader classes of uncertainty and confirming the robustness of the planning method.

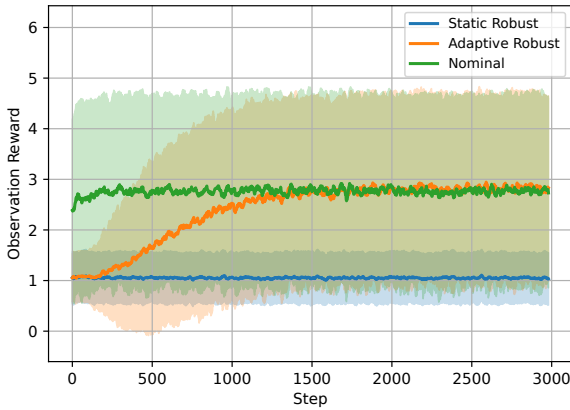
Figure 11 illustrates the temporal evolution of both observation and total rewards across the three planning strategies.

**Table 5** Modified parameters in Experiments 2

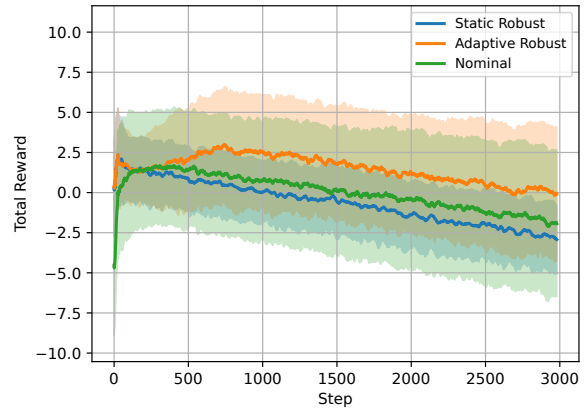
| Parameter                  | Description                                    | New Value / Setting           |
|----------------------------|--|-------------------------------|
| Observation model          | $o \sim \text{Gaussian or log-normal mixture}$ | Mixed Gaussian / log-normal   |
| Exposure model             | $x_p \sim \text{Gaussian mixture}$             | Mixed Gaussian                |
| Sensing cost               | $c_{\text{sense}}(a)$                          | $\{0.1, 0.1, 0.1, 0.1, 0.1\}$ |
| Immediate exposure penalty | $\lambda_{\text{imm}}$                         | -10.0                         |
| Persistent decay rate      | $\alpha$                                       | 0.99                          |
| Persistent exposure weight | $\lambda_{\text{pers}}$                        | 0.5                           |
| Cumulative exposure weight | $\lambda_{\text{cum}}$                         | 0.01                          |

**Table 6** Summary of Experiment 2 Results. Higher values are better for observation and total reward, while lower values are better for cumulative exposures.

| Planner         | Observation Reward $\uparrow$           | Cumulative Exposures $\downarrow$   | Total Reward $\uparrow$                 |
|-----------------|---|-------------------------------------|---|
| Adaptive Robust | $7334.50 \pm 936.78$                    | <b><math>77.29 \pm 26.41</math></b> | <b><math>4416.98 \pm 3101.26</math></b> |
| Nominal         | <b><math>8414.99 \pm 1069.28</math></b> | $109.11 \pm 39.93$                  | $-153.79 \pm 5352.14$                   |
| Static Robust   | $3210.33 \pm 297.09$                    | $87.62 \pm 11.74$                   | $-1998.17 \pm 1505.94$                  |



(a) Observation rewards over steps.



(b) Total rewards over steps.

**Fig. 11** Results of Experiment 2 comparing the reward evolution across three planning strategies. Both plots show 20-step moving-averaged results across random seeds. (a) Step-wise observation rewards. (b) Step-wise total rewards, including exposure penalties. Solid lines indicate the averaged performance across random seeds, and the shaded regions represent  $\pm 1$  standard deviation.

Similar to the Gaussian case in Experiment 1, the adaptive robust planner consistently maintains higher observation rewards while stabilizing total returns through balanced exploration and exposure control. In contrast, the nominal planner achieves higher observation rewards but yields lower overall performance under uncertain threat conditions. Figure 11b shows a gradual decrease in total rewards across all methods compared to Experiment 1. This trend results from the increased cumulative exposure weight  $\lambda_{\text{cum}}$ , which amplifies long-term penalty accumulation. Regardless of the parameter changes, the adaptive robust planner still outperforms the others and gradually recovers its total rewards as the ambiguity set refines over time.

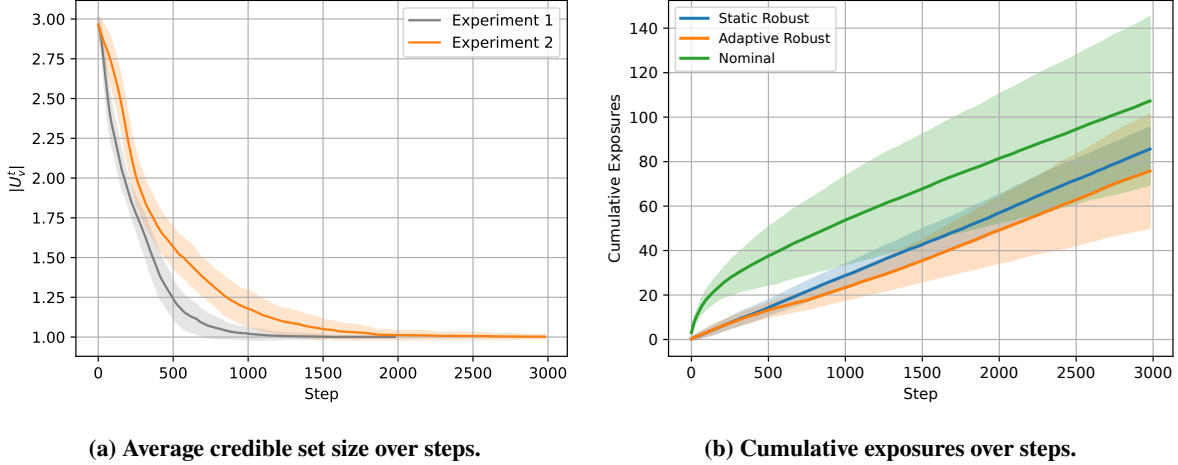


**Fig. 12 Results of Experiment 2.** (a) Step-wise changes in the credible set size  $|U_v^t|$  for the adaptive robust planner between Experiment 1 and Experiment 2. The results show how the adaptive-robust planner progressively reduces uncertainty under different experimental conditions. (b) Cumulative number of exposures over steps, compared across the three planning strategies. Both plots present 20-step moving-averaged results across random seeds. The solid lines denote the mean, and the shaded regions represent one standard deviation.

The underlying adaptive behavior is further analyzed in Figure 12. Figure 12a shows that the credible set size  $|U_v^t|$  steadily decreases as the adaptive planner gathers more informative observations, confirming effective uncertainty reduction under non-Gaussian distributions. Despite having the same graph size as in Experiment 1, the reduction progresses more slowly due to the broader coverage of the Gaussian mixture models, which makes distinguishing among threats more challenging. Correspondingly, Figure 12b demonstrates that this reduction in uncertainty translates to lower cumulative exposure compared to the nominal and static robust baselines. The overall variance in both rewards and exposures is higher than in Experiment 1, reflecting the wider spread of the observation and threat models used in Experiment 2.

Finally, Figure 13 compares the action selection distributions across the three planners, showing patterns similar to those in Experiment 1. The static robust policy consistently favors the safer Action D under uncertainty, while the adaptive robust planner initially exhibits similar conservative behavior but gradually shifts toward a more balanced selection as uncertainty decreases. These results demonstrate that the adaptive robust planner effectively adjusts its

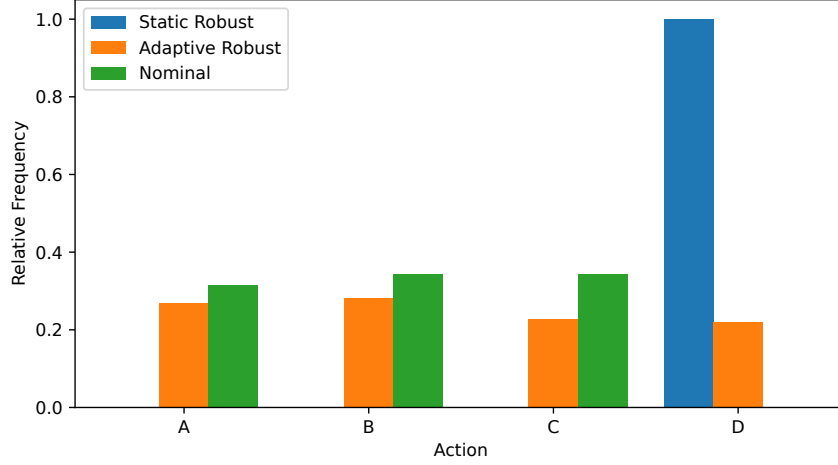


**Fig. 13** Distribution of sensing action selections across different policies in Experiment 2. Action labels (A–D) correspond to the mapped sense-action categories. Frequencies are normalized to show relative selection ratios.

sensing strategy while maintaining robustness across different threat conditions, even when the underlying threat models are non-Gaussian.

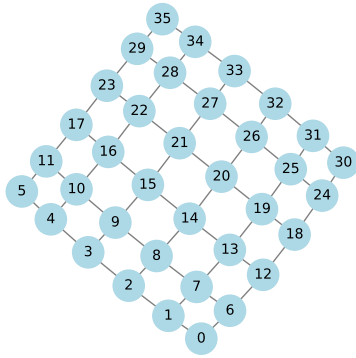
#### D. Experiment 3: Scalability across Network Topologies

To examine scalability, we test how the planner’s performance and computation time change with increasing network size and structural complexity. We test a variety of graph topologies that reflect practical ISR mission environments, ranging from regular grid-like layouts to irregular, hub-dominated, and modular regions. Assessing performance across these heterogeneous topologies allows us to measure robustness under diverse operational environments. The six representative topologies considered are illustrated in Figure 14.

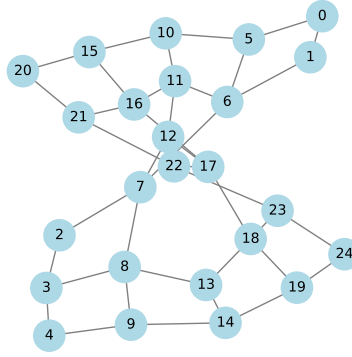
*Regular grid networks* ( $3 \times 4$ ,  $5 \times 5$ , and  $6 \times 6$ ) have a simple and regular structure, which allows direct comparison with the controlled setting of Experiment 1. *Grids with random edge deletions* ( $5 \times 5$  and  $6 \times 6$ ) introduce local connectivity disruptions, reflecting, e.g., terrain occlusions or restricted flight corridors [49, 50]. *Star networks*, composed of a central hub and 8 or 14 leaf nodes, are included to examine how the planner behaves in highly centralized hub-and-spoke structures. *Erdos–Renyi random graphs* with 15 and 30 nodes ( $p = 0.10, 0.15$ ) offer uniform random connectivity, serving as a baseline for comparison in networks without specific structural patterns. *Barabasi–Albert scale-free graphs* of comparable size ( $m = 2, 3$ ) represent networks where a few hubs have many connections. Finally, *stochastic block models (community)* with 20 and 35 nodes, containing 3 and 4 clusters ( $p_{\text{intra}} = 0.7$ ,  $p_{\text{inter}} = 0.05$  or  $0.03$ ), are used to test how well the planner adapts to modular networks with clear community structures.

Each experiment is repeated across 10 random seeds for each graph configuration and planner type (adaptive robust, static robust, and nominal) to ensure statistical consistency. All planners were tested in the same simulation environment as in Experiment 1. The exposure and reward settings were identical, but the simulation horizon was extended to 8000

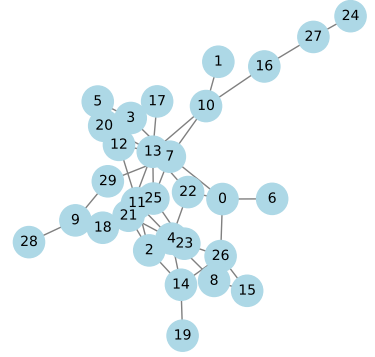




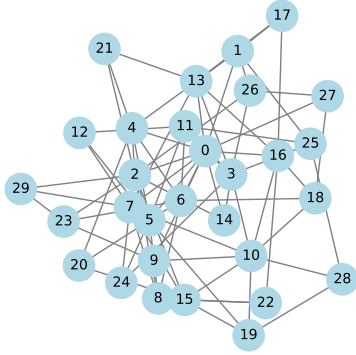
(a) Grid



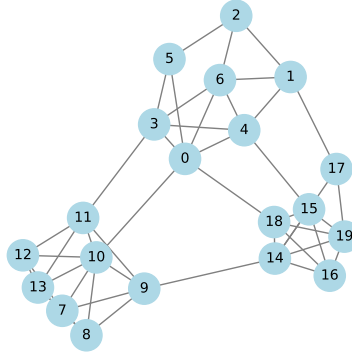
(b) Grid with edge deletions



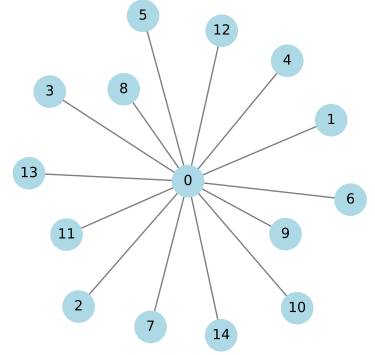
(c) Erdos-Renyi



(d) Barabasi-Albert



(e) Stochastic block model



(f) Star

**Fig. 14** Illustrations of the network topologies used in Experiment 3. Each structure differs in size and connectivity, representing diverse conditions for evaluating scalability.

time steps. Random seeds are fixed for graph generation and threat setup to ensure reproducibility while allowing for randomness in observations and exposures.

Table 7 summarizes the simulation results of Experiment 3, where all values are reported as mean  $\pm$  standard deviation across 10 random seeds. As shown in the table, the adaptive robust planner consistently achieved higher total rewards than both the nominal and static robust planners across all network topologies. For the observation rewards, values were generally similar within the same planner, regardless of the underlying graph type or size. This consistency arises because all simulations were run for 8000 steps, providing comparable opportunities for each planner to accumulate observable rewards. The nominal planner showed substantially higher cumulative exposure, indicating more aggressive and dangerous behavior than the other planners. As a result, its higher observation rewards are offset in the total reward value. This pattern is consistent with the findings from Figure 6, where the adaptive robust planner demonstrated superior long-term performance by maintaining a balanced trade-off between safety and efficiency. The result shows that the total reward also tended to increase with graph size. This trend occurs because, in larger networks, the novelty term remains high for longer as more nodes become available to explore. Furthermore, the adaptive robust planner exhibited smaller variance in both total rewards and cumulative exposures, confirming its stable and reliable performance across networks with different structures and scales.

Across all tested graph topologies and node sizes, the adaptive robust planner demonstrated stable and consistent convergence, which occurs when all credible sets become singletons (e.g.,  $|U_v^t| = 1$  for the reachable nodes). In a few runs, certain nodes failed to converge due to structural limitations in the network rather than a learning issue with the planner. These cases occurred when the graphs contained disconnected components, making some nodes unreachable from the main connected component. Because the graphs were randomly generated, such disconnected components appeared occasionally. After excluding structurally invalid cases, our adaptive robust planner successfully converged for all reachable nodes. The mean and standard deviation of the convergence steps increased gradually with graph size, indicating that the planner remains reliable across networks of different structures and scales.

Figure 15 illustrates how graph size and topology influence the performance of the adaptive robust planner. Distinct marker shapes represent different graph topologies, while the horizontal axis denotes the number of nodes in each graph. Each point corresponds to the number of steps required for the size of all credible sets to reach one ( $|U_v^t| = 1$ ) among the reachable nodes. The results indicate that, regardless of the network topology, the number of nodes is a key parameter that determines the adaptive planner’s efficiency. A clear linear relationship is observed between graph size and convergence steps, demonstrating that the proposed adaptive planner operates consistently across diverse graph structures. Each episode was limited to 8000 steps, yet even the slowest-converging case required only around 5200 steps to fully resolve all ambiguity sets.

**Table 7 Summary of Experiment 3 Results. Comparisons are valid only within each graph type and not across different topologies.**

| Graph Type               | Nodes | Planner         | Obs. Reward $\uparrow$                  | Cum. Exposure $\downarrow$           | Total Reward $\uparrow$                    |
|--------------------------|-------|-----------------|---|--------------------------------------|--|
| Barabasi-Albert          | 15    | Adaptive Robust | 26604.09 $\pm$ 228.80                   | <b>109.60 <math>\pm</math> 7.17</b>  | <b>641121.85 <math>\pm</math> 1991.10</b>  |
|                          |       | Nominal         | <b>27633.34 <math>\pm</math> 215.70</b> | 474.80 $\pm$ 103.36                  | 9686.63 $\pm$ 14999.06                     |
|                          |       | Static Robust   | 6376.57 $\pm$ 676.51                    | 365.00 $\pm$ 13.33                   | 10969.77 $\pm$ 2855.34                     |
|                          | 30    | Adaptive Robust | 25267.94 $\pm$ 237.34                   | <b>121.60 <math>\pm</math> 4.25</b>  | <b>155323.85 <math>\pm</math> 1247.38</b>  |
|                          |       | Nominal         | <b>27355.98 <math>\pm</math> 151.74</b> | 744.70 $\pm$ 123.64                  | 70484.12 $\pm$ 13970.15                    |
|                          |       | Static Robust   | 6234.28 $\pm$ 744.20                    | 365.70 $\pm$ 14.01                   | 105826.26 $\pm$ 2308.49                    |
| Stochastic Block Model   | 30    | Adaptive Robust | 25350.52 $\pm$ 361.47                   | <b>121.10 <math>\pm</math> 5.90</b>  | <b>146729.40 <math>\pm</math> 1296.92</b>  |
|                          |       | Nominal         | <b>27347.23 <math>\pm</math> 187.65</b> | 744.50 $\pm$ 158.72                  | 59647.03 $\pm$ 19560.29                    |
|                          |       | Static Robust   | 6182.58 $\pm$ 773.15                    | 365.70 $\pm$ 14.01                   | 96770.31 $\pm$ 4566.13                     |
|                          | 40    | Adaptive Robust | 24294.14 $\pm$ 320.70                   | <b>136.60 <math>\pm</math> 6.96</b>  | <b>218087.10 <math>\pm</math> 1372.49</b>  |
|                          |       | Nominal         | <b>27181.90 <math>\pm</math> 150.27</b> | 930.70 $\pm$ 119.53                  | 113903.51 $\pm$ 13890.50                   |
|                          |       | Static Robust   | 6187.70 $\pm$ 568.42                    | 365.90 $\pm$ 12.64                   | 172227.88 $\pm$ 2468.59                    |
| Erdos-Renyi              | 15    | Adaptive Robust | 26944.90 $\pm$ 567.93                   | <b>116.80 <math>\pm</math> 35.00</b> | <b>44870.10 <math>\pm</math> 21794.13</b>  |
|                          |       | Nominal         | <b>27699.09 <math>\pm</math> 273.14</b> | 435.60 $\pm$ 169.30                  | -3554.78 $\pm$ 15704.17                    |
|                          |       | Static Robust   | 6245.47 $\pm$ 691.76                    | 365.00 $\pm$ 13.33                   | -7520.53 $\pm$ 22919.71                    |
|                          | 30    | Adaptive Robust | 25589.12 $\pm$ 869.56                   | <b>119.00 <math>\pm</math> 9.63</b>  | <b>148749.01 <math>\pm</math> 51479.06</b> |
|                          |       | Nominal         | <b>27385.43 <math>\pm</math> 255.58</b> | 720.50 $\pm$ 220.94                  | 67701.03 $\pm$ 36151.77                    |
|                          |       | Static Robust   | 6134.88 $\pm$ 819.49                    | 365.70 $\pm$ 14.01                   | 98663.02 $\pm$ 52665.88                    |
| Grid                     | 12    | Adaptive Robust | 26999.01 $\pm$ 196.12                   | <b>102.90 <math>\pm</math> 7.71</b>  | <b>44345.51 <math>\pm</math> 2482.13</b>   |
|                          |       | Nominal         | <b>27689.68 <math>\pm</math> 163.95</b> | 441.90 $\pm$ 160.51                  | -10734.79 $\pm$ 22350.71                   |
|                          |       | Static Robust   | 6127.44 $\pm$ 815.71                    | 364.80 $\pm$ 13.06                   | -13145.22 $\pm$ 1443.97                    |
|                          | 25    | Adaptive Robust | 25687.31 $\pm$ 322.45                   | <b>128.60 <math>\pm</math> 22.19</b> | <b>121098.12 <math>\pm</math> 5810.31</b>  |
|                          |       | Nominal         | <b>27441.00 <math>\pm</math> 159.42</b> | 702.50 $\pm$ 172.20                  | 34449.63 $\pm$ 20104.99                    |
|                          |       | Static Robust   | 6184.44 $\pm$ 790.95                    | 364.50 $\pm$ 14.00                   | 64835.45 $\pm$ 2247.67                     |
|                          | 36    | Adaptive Robust | 24709.20 $\pm$ 333.65                   | <b>151.50 <math>\pm</math> 34.08</b> | <b>185971.11 <math>\pm</math> 4331.75</b>  |
|                          |       | Nominal         | <b>27251.40 <math>\pm</math> 180.25</b> | 861.80 $\pm$ 133.23                  | 85872.47 $\pm$ 15090.80                    |
|                          |       | Static Robust   | 6093.93 $\pm$ 724.04                    | 366.10 $\pm$ 12.60                   | 134456.16 $\pm$ 2058.68                    |
| Grid with Edge Deletions | 25    | Adaptive Robust | 25741.21 $\pm$ 145.88                   | <b>117.70 <math>\pm</math> 9.24</b>  | <b>132262.88 <math>\pm</math> 7148.92</b>  |
|                          |       | Nominal         | <b>27466.33 <math>\pm</math> 225.79</b> | 694.70 $\pm$ 209.91                  | 50786.09 $\pm$ 25616.49                    |
|                          |       | Static Robust   | 6044.33 $\pm$ 730.08                    | 368.10 $\pm$ 13.55                   | 80153.59 $\pm$ 8032.60                     |
|                          | 36    | Adaptive Robust | 25134.64 $\pm$ 1020.19                  | <b>126.20 <math>\pm</math> 13.41</b> | <b>194330.90 <math>\pm</math> 68213.77</b> |
|                          |       | Nominal         | <b>27359.72 <math>\pm</math> 283.59</b> | 683.50 $\pm$ 217.12                  | 118948.59 $\pm$ 52728.24                   |
|                          |       | Static Robust   | 5794.11 $\pm$ 1462.13                   | 367.60 $\pm$ 14.75                   | 144842.62 $\pm$ 72473.51                   |
| Star                     | 9     | Adaptive Robust | 27198.16 $\pm$ 207.06                   | <b>103.20 <math>\pm</math> 8.48</b>  | <b>32855.09 <math>\pm</math> 1494.85</b>   |
|                          |       | Nominal         | <b>27711.70 <math>\pm</math> 239.62</b> | 416.30 $\pm$ 144.04                  | -16254.38 $\pm$ 20902.36                   |
|                          |       | Static Robust   | 5593.48 $\pm$ 1759.26                   | 364.60 $\pm$ 13.28                   | -22579.18 $\pm$ 1664.92                    |
|                          | 15    | Adaptive Robust | 26628.59 $\pm$ 263.27                   | <b>109.80 <math>\pm</math> 9.41</b>  | <b>67126.14 <math>\pm</math> 1709.23</b>   |
|                          |       | Nominal         | <b>27689.59 <math>\pm</math> 232.86</b> | 401.50 $\pm$ 135.57                  | 22525.42 $\pm$ 17940.09                    |
|                          |       | Static Robust   | 6251.57 $\pm$ 1343.95                   | 365.00 $\pm$ 13.33                   | 14061.61 $\pm$ 1853.36                     |

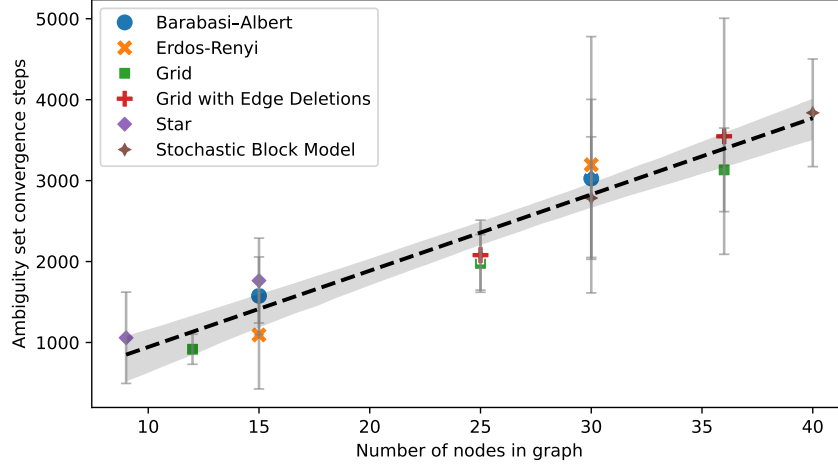


**Fig. 15** Each point represents the mean number of steps required for the ambiguity set  $U_t$  to converge (mean  $\pm$  std) across networks of different sizes and types. Error bars indicate one standard deviation over random seeds, and the dashed black line denotes the overall linear trend across all network types.

## VIII. Conclusion

### A. Summary

We present an adaptive RMDP framework for decision-making in an uncertain threat environment, where a single CCA performs repetitive surveillance missions within a partitioned ISR operation area. In addition, the framework is supported by theoretical guarantees on operator convergence, asymptotic optimality, and probabilistic safety, providing a rigorous foundation for its reliability under uncertainty. The proposed approach addresses the limitations of conventional RMDPs that rely on static ambiguity sets by incorporating a Bayesian inference-based mechanism to reduce ambiguity set sizes. This enables the agent to progressively update its threat model and refine its policy using observations collected during mission execution. Consequently, as the agent repeatedly monitors its assigned region, it naturally transitions from conservative to aggressive behaviors as the uncertainties are reduced.

The effectiveness of the proposed algorithm was demonstrated through three sets of experiments. The first experiment confirmed that the proposed adaptive robust planner exhibited the intended transition from conservative to efficient behavior as it accumulated environmental knowledge in a simple environment, while the second demonstrated generalization capability under non-Gaussian threat distributions. The third experiment evaluated adaptability and scalability across various graph sizes and topologies. The results showed that our adaptive robust planner achieved higher cumulative rewards and lower exposure risk than static robust and nominal planners, highlighting its advantage in leveraging accumulated observations to continuously improve policy during repetitive surveillance missions. Overall, the proposed method provides a decision-making structure that autonomously balances robustness and adaptivity in contested environments, offering a promising direction for reliable long-term surveillance under uncertainty.

## B. Limitations and Future Work

We plan to extend the current work in two primary directions, each motivated by limitations of the present work. First, the current adaptive RMDP framework is restricted to a single agent operating within a fixed region and does not account for interactions among multiple CCAs. To address this limitation, we will expand to a distributed, multi-agent environments. While the present work focuses on a single agent repeatedly conducting surveillance within its assigned region, actual ISR operations involve multiple agents operating in adjacent areas and interacting with one another. Future work will therefore consider information exchange, mutual trust modeling, and distributed decision-making structures to enable cooperative behavior among agents. In particular, under dynamically changing threat conditions or information asymmetry, mechanisms for region reassignment and policy synchronization will be investigated to enhance overall surveillance efficiency and system resilience. We aim to scale robustness of the adaptive RMDP approach to a distributed system level, improving its applicability in realistic CCA operating scenarios.

Second, the present study assumes fully autonomous operation and does not incorporate human intervention, which is a core aspect of practical CCA employment. Therefore, we will explore the integration of human involvement and intervention in the decision-making process. This direction reflects the fundamental concept of CCAs as autonomous teammates that operate in coordination with human pilots. Future studies will model various forms of human involvement in the decision-making process, ranging from soft interventions (e.g., the human provides guidance or modifies the autonomous policy), to hard overrides (e.g., the human operator directly takes control and alters the agent's actions). The effects of these interventions on policy adaptability, safety, and mission performance will be analyzed to assess the stability and learning characteristics of adaptive RMDP structures under human intervention. Furthermore, research will investigate decision-making architectures that can effectively integrate human high-level judgments from a human operator with autonomous computational reasoning, establishing the foundation for safe and reliable human-machine collaboration in future ISR missions.

## A. Appendix: Proofs of Section VI.C

*Proof of Theorem 1.* By Assumption 1, the one-step reward is bounded, so each  $\mathcal{T}_{\text{rob}}^t(\omega)$  maps  $\mathcal{B}$  onto itself. By Assumption 2, the operators are  $\gamma$ -contractions with a common  $\gamma \in (0, 1)$ . Let  $V, W \in \mathcal{B}$ , that is, bounded real-valued functions on  $\mathcal{S}'$ . Since  $\|\mathcal{T}_{\text{rob}}^t V - \mathcal{T}_{\text{rob}}^t W\|_{\infty} \leq \gamma \|V - W\|_{\infty}$  for all  $t$  and  $\mathcal{T}_{\text{rob}}^t \rightarrow \mathcal{T}_{\infty}$  uniformly on bounded sets, taking  $t \rightarrow \infty$  gives  $\|\mathcal{T}_{\infty} V - \mathcal{T}_{\infty} W\|_{\infty} \leq \gamma \|V - W\|_{\infty}$ .

Let  $\Omega_0$  be the event of probability one on which the above uniform convergence condition holds. Fix  $\omega \in \Omega_0$ . For this fixed  $\omega$ , all quantities are deterministic. Let  $V^*(\omega)$  be the unique fixed point of  $\mathcal{T}_{\infty}(\omega)$  on  $\mathcal{B}$  by Banach's fixed-point theorem. Uniform boundedness of rewards implies  $\|V^*(\omega)\|_{\infty} \leq R_{\max}/(1-\gamma)$  and, inductively,  $\sup_t \|V_t(\omega)\|_{\infty} \leq$

$R_{\max}/(1 - \gamma)$ . Let  $M := R_{\max}/(1 - \gamma)$  and  $B_M := \{V \in \mathcal{B} : \|V\|_{\infty} \leq M\}$ . Then, for all  $t$ ,

$$\begin{aligned}
\|V_{t+1}(\omega) - V^{\star}(\omega)\|_{\infty} &= \|\mathcal{T}_{\text{rob}}^t(\omega)V_t(\omega) - \mathcal{T}_{\infty}(\omega)V^{\star}(\omega)\|_{\infty} \\
&= \|\mathcal{T}_{\text{rob}}^t(\omega)V_t(\omega) - \mathcal{T}_{\infty}(\omega)V_t(\omega) + \mathcal{T}_{\infty}(\omega)V_t(\omega) - \mathcal{T}_{\infty}(\omega)V^{\star}(\omega)\|_{\infty} \\
&\leq \|\mathcal{T}_{\text{rob}}^t(\omega)V_t(\omega) - \mathcal{T}_{\infty}(\omega)V_t(\omega)\|_{\infty} + \|\mathcal{T}_{\infty}(\omega)V_t(\omega) - \mathcal{T}_{\infty}(\omega)V^{\star}(\omega)\|_{\infty},
\end{aligned} \tag{31}$$

where the last inequality is by the triangle inequality. Using the contraction property of  $\mathcal{T}_{\infty}(\omega)$ , we have

$$\|\mathcal{T}_{\infty}(\omega)V_t(\omega) - \mathcal{T}_{\infty}(\omega)V^{\star}(\omega)\|_{\infty} \leq \gamma \|V_t(\omega) - V^{\star}(\omega)\|_{\infty}. \tag{32}$$

For the first term, define the uniform deviation as

$$\varepsilon_t(\omega) := \sup_{V \in B_M} \|\mathcal{T}_{\text{rob}}^t(\omega)V - \mathcal{T}_{\infty}(\omega)V\|_{\infty}. \tag{33}$$

Since  $V_t(\omega) \in B_M$ , we have

$$\|\mathcal{T}_{\text{rob}}^t(\omega)V_t(\omega) - \mathcal{T}_{\infty}(\omega)V_t(\omega)\|_{\infty} \leq \varepsilon_t(\omega). \tag{34}$$

Combining (31) and (32) yields

$$\|V_{t+1}(\omega) - V^{\star}(\omega)\|_{\infty} \leq \gamma \|V_t(\omega) - V^{\star}(\omega)\|_{\infty} + \varepsilon_t(\omega). \tag{35}$$

Denoting  $x_t(\omega) := \|V_t(\omega) - V^{\star}(\omega)\|_{\infty}$ , we obtain

$$x_{t+1}(\omega) \leq \gamma x_t(\omega) + \varepsilon_t(\omega). \tag{36}$$

By uniform convergence on  $B_M$ ,  $\varepsilon_t(\omega) \rightarrow 0$ . The recursion  $x_{t+1} \leq \gamma x_t + \varepsilon_t$  then yields

$$x_t(\omega) \leq \gamma^t x_0(\omega) + \sum_{k=0}^{t-1} \gamma^{t-1-k} \varepsilon_k(\omega) \rightarrow 0, \tag{37}$$

since  $\gamma^t \rightarrow 0$  and the weighted sum vanishes as  $\varepsilon_t(\omega) \rightarrow 0$ . Hence  $V_t(\omega) \rightarrow V^{\star}(\omega)$  for all  $\omega \in \Omega_0$ .  $\square$

*Proof of Corollary 1.* By Assumption 5, each  $f_{v,a}$  is continuous on compact set  $\Theta$ , hence uniformly continuous. Since  $U_v^t \rightarrow \{\theta_v^{\star}\}$  in the PK sense by Assumption 4, and  $f_{v,a}$  is continuous, the minimum over  $U_v^t$  varies continuously as the

set shrinks to  $\{\theta_v^\star\}$ . Thus, for every  $(v, a)$ ,

$$\min_{\theta \in U_v^t} f_{v,a}(\theta) \longrightarrow f_{v,a}(\theta_v^\star) \quad \text{almost surely.} \quad (38)$$

For the transition term, fix  $s, a$  with  $v = v(s, a)$ . The maps

$$\theta \mapsto \mathbb{E}_{P(\cdot|s,a;\theta)}[V(S')] \quad \text{and} \quad P \mapsto \mathbb{E}_P[V(S')] \quad (39)$$

are continuous for bounded  $V$  and finite  $S'$ . Since  $U_{s,a}^t = \phi_{s,a}(U_v^t)$  and  $\phi_{s,a}$  is continuous, the induced ambiguity sets  $U_{s,a}^t$  converge in the PK sense to  $U_{s,a}^\infty := \{\phi_{s,a}(\theta_v^\star)\}$ . Therefore,

$$\min_{P \in U_{s,a}^t} \mathbb{E}_P[V(S')] \longrightarrow \mathbb{E}_{P^\star(\cdot|s,a)}[V(S')] \quad \text{a.s.} \quad (40)$$

Combining the stage and transition limits, we obtain for any bounded  $B \subset \mathcal{B}$ , we have that

$$\sup_{V \in B} \|\mathcal{T}_{\text{rob}}^t V - \mathcal{T}_{\text{nom}}^{\theta^\star} V\|_\infty \xrightarrow[t \rightarrow \infty]{} 0 \quad \text{a.s.} \quad (41)$$

Assumptions 1 and 2 imply each  $\mathcal{T}_{\text{rob}}^t$  is a  $\gamma$ -contraction with common modulus  $\gamma \in (0, 1)$ . Theorem 1 applies and yields  $V_t \rightarrow V_{\text{nom}}^\star$  almost surely. Since  $V_t \rightarrow V_{\text{nom}}^\star$  and the transition models converge, the corresponding one-step lookahead values  $Q_t$  also converge pointwise to  $Q_{\text{nom}}^\star$ . If the maximizer is unique at every state for  $Q_{\text{nom}}^\star$ , the greedy selector is single valued for all large  $t$ , hence  $\pi_t \rightarrow \pi_{\text{nom}}^\star$ .  $\square$

*Proof of Proposition 1.* On the event  $\mathcal{E}_t$  we have  $\theta_v^\star \in U_v^t$  for all  $v$ . By definition of the ambiguity set  $U_{s,a}^t$  and because each transition model depends on its local parameter, for every  $(s, a)$  with  $v = v(s, a)$ ,

$$P^\star(\cdot | s, a) = \phi_{s,a}(\theta_v^\star) \in \phi_{s,a}(U_v^t) = U_{s,a}^t. \quad (42)$$

Hence, on  $\mathcal{E}_t$ , we have  $P^\star \in U^t := \prod_{(s,a)} U_{s,a}^t$ . Therefore, still on  $\mathcal{E}_t$  and for every  $s$ ,

$$V_{P^\star}^{\pi_t}(s) \geq \min_{P \in U^t} V_P^{\pi_t}(s). \quad (43)$$

Taking probabilities and using that the inequality holds for all  $s$  simultaneously on  $\mathcal{E}_t$  gives

$$\mathbb{P}\left(\forall s \in S' : V_{P^\star}^{\pi_t}(s) \geq \min_{P \in U^t} V_P^{\pi_t}(s)\right) \geq \mathbb{P}(\mathcal{E}_t) = 1 - \delta_t. \quad (44)$$

## Acknowledgements

This project was supported by NSF IUCRC Phase I: Center for Autonomous Air Mobility and Sensing (CAAMS) Award No. 2137195. The authors also thank Mengmeng Li from École Polytechnique Fédérale de Lausanne (EPFL) for valuable discussions and feedback that helped improve the theoretical components of this work.

## References

- [1] Choi, J., and Li, M. Z., “Adaptive Robust Markov Decision Process for Wide-Area Surveillance with Collaborative Combat Aircraft,” 2026. To be presented at the 2026 AIAA SciTech Forum, Orlando, FL, USA.
- [2] Gunzinger, C. M. A., Stutzriem, M. G. L. A., and Sweetman, B., “The Need for Collaborative Combat Aircraft for Disruptive Air Warfare,” Tech. rep., Mitchell Institute for Aerospace Studies, Arlington, VA, February 2024.
- [3] Penney, H. R., “Five Imperatives for Developing Collaborative Combat Aircraft for Teaming Operations,” Tech. rep., The Mitchell Institute for Aerospace Studies, Air & Space Forces Association, Arlington, VA, 10 2022.
- [4] DiMascio, J., “U.S. Air Force Collaborative Combat Aircraft (CCA),” Tech. Rep. IF12740, Congressional Research Service, 2024. URL <https://crsreports.congress.gov/product/pdf/IF/IF12740>, accessed on May 21, 2025.
- [5] Adamy, D. L., *Introduction to Electronic Warfare Modeling and Simulation*, Scitech Publishing, Raleigh, NC, 2006.
- [6] Ma, C., Guleria, Y., Alam, S., and Li, M. Z., “Deep Reinforcement Learning-Based Air Traffic Flow Coordination in Flow-Centric Airspace,” *Advanced Engineering Informatics*, Vol. 65, 2025, p. 103342. <https://doi.org/https://doi.org/10.1016/j.aei.2025.103342>.
- [7] Choi, J., and Ahn, J., “Uncertainty-Aware Autonomous Mars Landing Guidance With Curriculum Reinforcement Learning,” *AIAA SCITECH 2025 Forum*, 2025. <https://doi.org/10.2514/6.2025-1933>.
- [8] Koch, W., Mancuso, R., West, R., and Bestavros, A., “Reinforcement Learning for UAV Attitude Control,” *ACM Trans. Cyber-Phys. Syst.*, Vol. 3, No. 2, 2019. <https://doi.org/10.1145/3301273>.
- [9] Kirschner, J., Bogunovic, I., Jegelka, S., and Krause, A., “Distributionally robust Bayesian optimization,” *International Conference on Artificial Intelligence and Statistics*, 2020, pp. 2174–2184. <https://doi.org/10.48550/ARXIV.2002.09038>.
- [10] Iyengar, G., “Robust dynamic programming,” *Mathematics of Operations Research*, Vol. 30, No. 2, 2005, pp. 257–280. <https://doi.org/10.1287/moor.1040.0129>.
- [11] Nilim, A., and El Ghaoui, L., “Robust Control of Markov Decision Processes with Uncertain Transition Matrices,” *Operations Research*, Vol. 53, No. 5, 2005, pp. 780–798. <https://doi.org/10.1287/opre.1050.0216>.



- [12] Wiesemann, W., Kuhn, D., and Rustem, B., “Robust Markov decision processes,” *Mathematics of Operations Research*, Vol. 38, No. 1, 2013, pp. 153–183. <https://doi.org/10.1287/moor.1120.0566>.
- [13] Choi, J., Stagg, G., Peterson, C. K., and Li, M. Z., “Bi-Level Route Optimization and Path Planning with Hazard Exploration,” *arXiv preprint arXiv:2503.24044*, 2025. URL <https://arxiv.org/abs/2503.24044>.
- [14] Choi, J., and Li, M. Z., “Bandit-Enabled Dynamic Vehicle Dispatch and Routing in Hazardous Environments,” *AIAA AVIATION FORUM AND ASCEND 2025*, 2025. <https://doi.org/10.2514/6.2025-3411>.
- [15] Choi, J., and Li, M. Z., “Autonomous Air-Ground Vehicle Operations Optimization in Hazardous Environments: A Multi-Armed Bandit Approach,” *arXiv preprint arXiv:2508.08217*, 2025. URL <https://arxiv.org/abs/2508.08217>.
- [16] Sun, S., Qi, M., and Shen, Z.-J. M., “Online MDP with Prototypes Information: A Robust Adaptive Approach,” *Proceedings of the AAAI Conference on Artificial Intelligence*, Vol. 39, 2025, pp. 20717–20724. <https://doi.org/10.1609/aaai.v39i19.34283>.
- [17] Chizek, J. G., “Military Transformation: Intelligence, Surveillance and Reconnaissance,” Tech. Rep. ADA469293, Congressional Research Service, Library of Congress, Washington, D.C., January 2003. URL <https://apps.dtic.mil/sti/pdfs/ADA469293.pdf>.
- [18] Smagh, N. S., “Intelligence, Surveillance, and Reconnaissance Design for Great Power Competition,” Tech. Rep. AD1114211, Congressional Research Service, Washington, D.C., June 2020. URL <https://apps.dtic.mil/sti/pdfs/AD1114211.pdf>.
- [19] Department of the Air Force, “Air Force Doctrine Note 25-1: Artificial Intelligence,” Tech. rep., Apr. 2025. URL <https://www.doctrine.af.mil/Operational-Level-Doctrine/AFDN-25-1-Artificial-Intelligence/>.
- [20] Cheng, H., Conway, E., Heggedahl, T., Morgan, J., and Schlessman, B., “Explore AI and machine learning for future ISR collection planning and management,” *Artificial Intelligence and Machine Learning for Multi-Domain Operations Applications IV*, Vol. 12113, edited by T. Pham and L. Solomon, International Society for Optics and Photonics, SPIE, 2022, p. 1211313. <https://doi.org/10.1117/12.2619117>.
- [21] Jing, T., Wang, W., Wang, T., Li, X., and Zhou, X., “Dynamic Control Scheme of Multiswarm Persistent Surveillance in a Changing Environment,” *Computational Intelligence and Neuroscience*, Vol. 2019, No. 1, 2019, p. 6025657. <https://doi.org/10.1155/2019/6025657>.
- [22] Nigam, N., and Kroo, I., “Persistent Surveillance Using Multiple Unmanned Air Vehicles,” *2008 IEEE Aerospace Conference*, 2008, pp. 1–14. <https://doi.org/10.1109/AERO.2008.4526242>.
- [23] Lappas, V., Shin, H.-S., Tsourdos, A., Lindgren, D., Bertrand, S., Marzat, J., Piet-Lahanier, H., Daramouskas, Y., and Kostopoulos, V., “Autonomous Unmanned Heterogeneous Vehicles for Persistent Monitoring,” *Drones*, Vol. 6, No. 4, 2022. <https://doi.org/10.3390/drones6040094>.
- [24] Wu, Y., Wu, S., and Hu, X., “Cooperative Path Planning of UAVs & UGVs for a Persistent Surveillance Task in Urban Environments,” *IEEE Internet of Things Journal*, Vol. 8, No. 6, 2021, pp. 4906–4919. <https://doi.org/10.1109/JIOT.2020.3030240>.

- [25] Lin, X., Yazıcıoğlu, Y., and Aksaray, D., “Robust Planning for Persistent Surveillance With Energy-Constrained UAVs and Mobile Charging Stations,” *IEEE Robotics and Automation Letters*, Vol. 7, No. 2, 2022, pp. 4157–4164. <https://doi.org/10.1109/LRA.2022.3146938>.
- [26] Egorov, M., Kochenderfer, M., and Uudmae, J., “Target Surveillance in Adversarial Environments Using POMDPs,” *Proceedings of the AAAI Conference on Artificial Intelligence*, Vol. 30, No. 1, 2016.
- [27] Temizer, S., Kochenderfer, M., Kaelbling, L., Lozano-Perez, T., and Kuchar, J., “Collision Avoidance for Unmanned Aircraft using Markov Decision Processes\*,” *AIAA Guidance, Navigation, and Control Conference*, 2010.
- [28] Durrant-Whyte, H., Roy, N., and Abbeel, P., *Unmanned Aircraft Collision Avoidance Using Continuous-State POMDPs*, 2012, pp. 1–8.
- [29] Yu, X., Zhou, X., and Zhang, Y., “Collision-free trajectory generation for UAVs using Markov decision process,” *2017 International Conference on Unmanned Aircraft Systems (ICUAS)*, 2017, pp. 56–61. <https://doi.org/10.1109/ICUAS.2017.7991332>.
- [30] Ong, H. Y., and Kochenderfer, M. J., “Markov Decision Process-Based Distributed Conflict Resolution for Drone Air Traffic Management,” *Journal of Guidance, Control, and Dynamics*, Vol. 40, No. 1, 2017, pp. 69–80. <https://doi.org/10.2514/1.G001822>.
- [31] Tang, Y., and Xu, Y., “Multi-Agent Deep Reinforcement Learning for Solving Large-scale Air Traffic Flow Management Problem: A Time-Step Sequential Decision Approach,” *2021 IEEE/AIAA 40th Digital Avionics Systems Conference (DASC)*, 2021, pp. 1–10. <https://doi.org/10.1109/DASC52595.2021.9594329>.
- [32] Spatharis, C., Blekas, K., Bastas, A., Kravaris, T., and Vouros, G. A., “Collaborative multiagent reinforcement learning schemes for air traffic management,” *2019 10th International Conference on Information, Intelligence, Systems and Applications (IISA)*, 2019, pp. 1–8. <https://doi.org/10.1109/IISA.2019.8900719>.
- [33] Balachandran, S., and Atkins, E., “Markov Decision Process Framework for Flight Safety Assessment and Management,” *Journal of Guidance, Control, and Dynamics*, Vol. 40, No. 4, 2017, pp. 817–830. <https://doi.org/10.2514/1.G001743>.
- [34] Nilim, A., Ghaoui, L., Hansen, M., and Duong, V., “Trajectory-based air traffic management (TB-ATM) under weather uncertainty,” *4th USA/EUROPE ATM R&D Seminar*, 2001.
- [35] Suilen, M., Badings, T., Bovy, E. M., Parker, D., and Jansen, N., *Robust Markov Decision Processes: A Place Where AI and Formal Methods Meet*, Springer Nature Switzerland, Cham, 2025, pp. 126–154. [https://doi.org/10.1007/978-3-031-75778-5\\_7](https://doi.org/10.1007/978-3-031-75778-5_7).
- [36] Wang, Y., and Zou, S., “Policy Gradient Method For Robust Reinforcement Learning,” *Proceedings of the 39th International Conference on Machine Learning*, Proceedings of Machine Learning Research, Vol. 162, edited by K. Chaudhuri, S. Jegelka, L. Song, C. Szepesvari, G. Niu, and S. Sabato, PMLR, 2022, pp. 23484–23526. URL <https://proceedings.mlr.press/v162/wang22at.html>.

- [37] Le Tallec, Y., “Robust, Risk-Sensitive, and Data-Driven Control of Markov Decision Processes,” Ph.D. thesis, Massachusetts Institute of Technology, 2007. URL <http://hdl.handle.net/1721.1/38598>.
- [38] Li, M., Kuhn, D., and Sutter, T., “Towards Optimal Offline Reinforcement Learning,” *arXiv preprint arXiv:2503.12283*, 2025. URL <https://arxiv.org/abs/2503.12283>.
- [39] Blanchet, J., Lu, M., Zhang, T., and Zhong, H., “Double Pessimism is Provably Efficient for Distributionally Robust Offline Reinforcement Learning: Generic Algorithm and Robust Partial Coverage,” *Advances in Neural Information Processing Systems*, Vol. 36, edited by A. Oh, T. Naumann, A. Globerson, K. Saenko, M. Hardt, and S. Levine, Curran Associates, Inc., 2023, pp. 66845–66859.
- [40] Zhao, W., Queralta, J. P., and Westerlund, T., “Sim-to-Real Transfer in Deep Reinforcement Learning for Robotics: a Survey,” *2020 IEEE Symposium Series on Computational Intelligence (SSCI)*, 2020, pp. 737–744. <https://doi.org/10.1109/SSCI47803.2020.9308468>.
- [41] Dong, J., Li, J., Wang, B., and Zhang, J., “Online Policy Optimization for Robust Markov Decision Process,” *Proceedings of the Fortieth Conference on Uncertainty in Artificial Intelligence*, JMLR.org, 2024.
- [42] Akbarzadeh, V., Gagne, C., Parizeau, M., Argany, M., and Mostafavi, M. A., “Probabilistic Sensing Model for Sensor Placement Optimization Based on Line-of-Sight Coverage,” *IEEE Transactions on Instrumentation and Measurement*, Vol. 62, No. 2, 2013, pp. 293–303. <https://doi.org/10.1109/TIM.2012.2214952>.
- [43] Pierson, A., Figueiredo, L. C., Pimenta, L. C., and Schwager, M., “Adapting to sensing and actuation variations in multi-robot coverage,” *Int. J. Rob. Res.*, Vol. 36, No. 3, 2017, p. 337–354. <https://doi.org/10.1177/0278364916688103>.
- [44] Aubin, J.-P., and Frankowska, H., *Set-Valued Analysis*, 1<sup>st</sup> ed., Modern Birkhäuser Classics, Birkhäuser Boston, Boston, MA, 2009. <https://doi.org/10.1007/978-0-8176-4848-0>.
- [45] Puterman, M. L., *Markov Decision Processes: Discrete Stochastic Dynamic Programming*, 1<sup>st</sup> ed., John Wiley & Sons, Inc., USA, 1994.
- [46] Billingsley, P., *Convergence of Probability Measures*, 2<sup>nd</sup> ed., Wiley Series in Probability and Statistics, John Wiley & Sons, 1999. <https://doi.org/10.1002/9780470316962>.
- [47] Billingsley, J. B., *Low-Angle Radar Land Clutter: Measurements and Empirical Models*, Institution of Engineering and Technology, London, UK, 2002.
- [48] Ward, K., Tough, R., and Watts, S., *Sea Clutter: Scattering, the K Distribution and Radar Performance*, 2<sup>nd</sup> ed., Radar, Sonar and Navigation, The Institution of Engineering and Technology, 2013.
- [49] Krzywdziński, K., and Rybarczyk, K., “Geometric Graphs with Randomly Deleted Edges - Connectivity and Routing Protocols,” *Mathematical Foundations of Computer Science 2011*, edited by F. Murlak and P. Sankowski, Springer Berlin Heidelberg, Berlin, Heidelberg, 2011, pp. 544–555.

- [50] Seymour, P., and Welsh, D., “Percolation Probabilities on the Square Lattice,” *Advances in Graph Theory*, Annals of Discrete Mathematics, Vol. 3, edited by B. Bollobás, Elsevier, 1978, pp. 227–245. [https://doi.org/https://doi.org/10.1016/S0167-5060\(08\)70509-0](https://doi.org/https://doi.org/10.1016/S0167-5060(08)70509-0).